University of Alberta

DEVELOPMENT OF A BINDING-INDUCED DNA NANOSENSOR BASED ON FLUORESCENCE RESONANCE ENERGY TRANSFER

by

Xukun Li

A thesis submitted to the Faculty of Graduate Studies and Research

in partial fulfillment of the requirements for the degree of

Master of Science

Department of Chemistry

Spring 2013

Edmonton, Alberta

ABSTRACT

This thesis describes a binding-induced DNA nanosensor and its application to homogeneous detection of DNA and proteins. This nanosensor was based on the binding-induced assembly of fluorescently labeled DNA on the DNA-functionalized quantum dots, resulting in fluorescence resonance energy transfer (FRET) between the quantum dots (605 QDs) and the fluorescent dye (Cy5). The sensor was applied to the detection of single-nucleotide polymorphism (SNP) in the *p53* gene sequence and the detection of platelet derived growth factor, with pM detection limits. This strategy can be applied to developing assays for a wide range of targets by functionalizing the surface of quantum dots with appropriate affinity ligands (e.g., aptamers and antibodies).

ACKNOWLEDGEMENTS

I would like to thank my research supervisor, Dr. X. Chris Le, for his encouragement, guidance, support and patience throughout this project. He guided me to shape thorough critical thinking and form innovative ideas with his enthusiasm for research.

I would like to express my gratitude to my committee members, Dr. Robert E. Campbell and Dr. Hongquan Zhang, for their thoughtful suggestions and comments on my work and thesis.

I would also like to express thanks to Dr. Lingling Yang, Dr. Zhixin Wang, and Ms. Brittany Dever for their advice on this work.

I appreciate all the help from my other group members of the Division of Analytical and Environmental Toxicology and thank them for their support and encouragement during my study. I acknowledge the support of the Graduate Teaching Assistantship and the Graduate Research Assistantship from the Department of Chemistry.

And last but not least, I thank my parents and friends for all their love, support and endless encouragement towards me.

TABLE OF CONTENTS

LIST OF TABLES

LIST OF FIGURES

LIST OF ABBREVIATIONS

BINDA	binding-induced DNA assembly
cDNA	complementary deoxyribonucleic acid evolution of ligands by exponential enrichment
CE-SELEX	capillary electrophoresis systematic evolution of ligands by exponential enrichment
CS-SELEX	cell specific systematic evolution of ligands by exponential enrichment
DNA	deoxyribonucleic acid
ECM	extracellular matrix
ELISA	enzyme-linked immunosorbent assay
FISH	fluorescence in situ hybridization
FRET	fluorescence resonance energy transfer
LOD	limit of detection
M-SELEX	microfluidics systematic evolution of ligands by exponential enrichment
NIR	near infrared
ODGF	osteosarcoma-derived growth factor
PBS	phosphate buffered saline
PDGF	platelet-derived growth factor
PDGFR	platelet-derived growth factor receptor
Q	quantum yield
QD	quantum dot

RNA	ribonucleic acid
RTK	real-time kinematic
SELEX	systematic evolution of ligands by exponential enrichment
SNP	single-nucleotide polymorphism
TECS-SELEX	target expressed on cell surface systematic evolution of ligands by exponential enrichment

Chapter 1: Introduction

1.1 Fluorescence resonance energy transfer (FRET)

Fluorescence resonance energy transfer (FRET) is a mechanism describing the energy transfer from an excited donor molecule to an acceptor molecule without emission of a photon through nonradiative dipole-dipole coupling [1]. An experiment based on FRET typically involves two or more fluorophores, which should include at least one donor and one acceptor [2]. When the incident light excites the donor molecule, the excited donor emits photons which are instantly absorbed by the acceptor in close proximity. The process of energy transfer can be explained by the Jablonski schematic (Figure 1.1) which illustrates the electronic states of a molecule and the transitions between them. In the presence of a donor–acceptor pair, when the excitation light excites the donor, its electrons jump from the ground state (S0) to an excited state (S1, S2, S3, etc.). These electrons at higher excited states (e.g. S2, S3) can return to the lowest excited state (S1), as well as electrons at S1 to S0. Meanwhile, energy is released during this process. The released energy is transferred from the donor to the acceptor, which excite the S0 state electrons of the acceptor to excited states. The excited electrons in the acceptor molecule transit from S1 to S0 and release the photon of light, which is detectable. The wavelength of the emitted light is longer than the exciting wavelength.

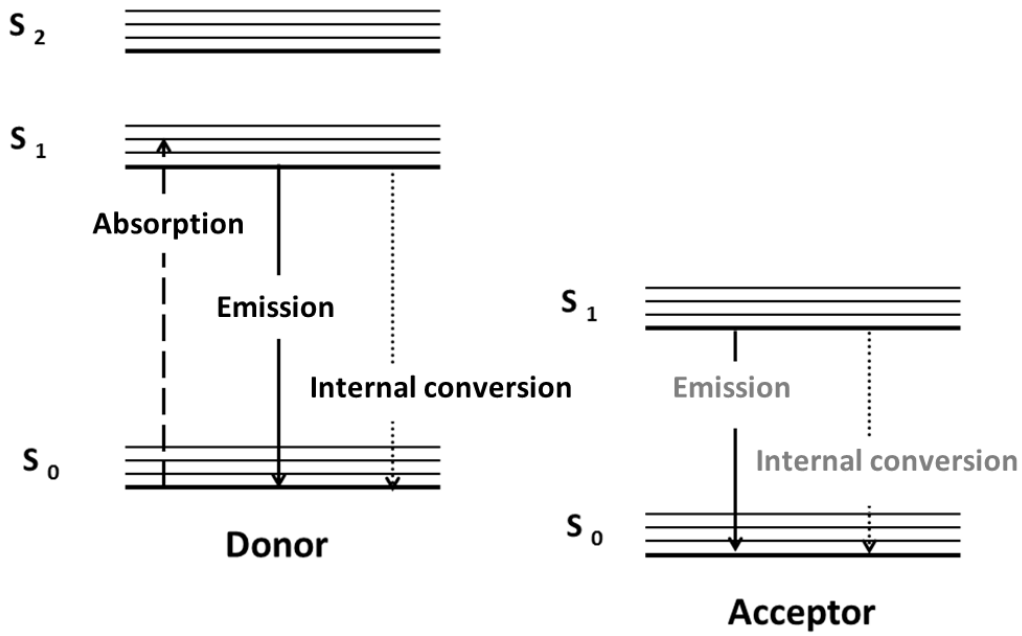

Figure 1.1 Jablonski schematic for explanation of fluorescence resonance energy transfer (FRET).

1.1.1 Parameters of FRET

For the one-to-one donor acceptor configuration, Figure 1.2 describes the competition among the decay as donor fluorescence and energy transfer between donor and acceptor and the decay of the excitation energy when the donor molecule is excited at the appropriate wavelength [3].

Based on Figure 1.2, several essential parameters will be introduced as follows:

- **Donor quantum yield**

The definition of quantum yield ($\boldsymbol{\Phi}$) of the donor is the ratio of the number of photons emitted to the number absorbed.

In the presence of transfer, the donor quantum yield ($\boldsymbol{\Phi_{DA}}$) is:

$$\boldsymbol{\Phi_{DA} = K_D / (K_T + K_D + K_{DNR})} \quad (1\text{-}1)$$

In the absence of transfer, the donor quantum yield ($\boldsymbol{\Phi_D}$) is:

$$\boldsymbol{\Phi_D = K_D / (K_D + K_{DNR})} \quad (1\text{-}2)$$

where $\boldsymbol{K_D}$ is the radiative decay constant of the donor in the absence of the acceptor, $\boldsymbol{K_T}$ is the rate constant of nonradiative energy transfer between donor and acceptor, and $\boldsymbol{K_{DNR}}$ is the nonradiative decay constant.

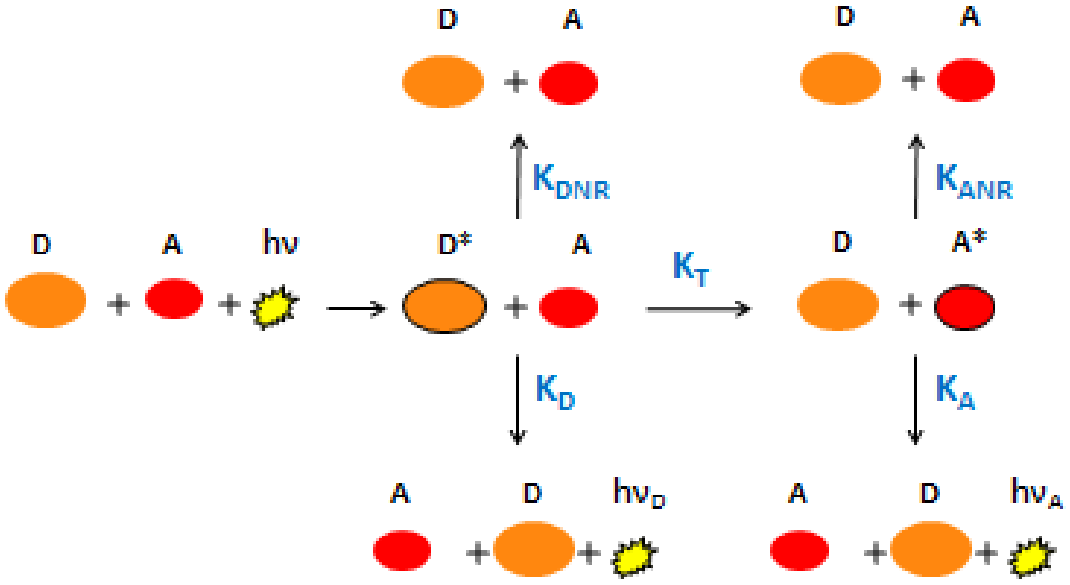

Figure 1.2 The schematic of competition among the decay as donor fluorescence and energy transfer between donor and acceptor and the decay of the excitation energy.

D represents the donor probe and ***A*** represents the acceptor probe, $h\nu$, $h\nu_D$ and $h\nu_A$ are photon energies of the donor excitation, donor fluorescence and of the acceptor fluorescence, respectively. K_D and K_A are the radiative decays of the donor in the absence of the acceptor and in the presence of the acceptor. K_T is the rate of nonradiative energy transfer between donor and acceptor. K_{DNR} and K_{ANR} are nonradiative decay constants.

- **Förster distance**

R_0 is the Förster distance of this pair of donor and acceptor, at which the efficiency of energy transfer is 50% [4], and which can be calculated for a given FRET system. The typical value of R_0 is 10–50 Å.

$$R_0 = [9000\ (\ln 10)\ \kappa^2\ \Phi_d\ J / 128\ \Pi^5\ n^4\ Na_v]^{1/6} \quad (1\text{-}3)$$

In Equation 1-3, Φ_d is the quantum yield of the donor, n is the refractive index of the medium and is generally assumed to be 1.4 (range 1.33–1.6) for liquid, Na_v is Avogadro's number (Na_v = 6.02 × 10^{23} per mole), κ^2 is the orientation factor and J is the overlap integral.

According to Equation 1-3, the distance R_0 is affected by the donor quantum yield, the index of refraction, the overlap between donor emission and acceptor absorption spectra, and the orientation of the dipoles.

- **Kappa square**

Kappa square is the orientation factor, which is defined as：

$$\kappa^2 = (\cos\theta_T - 3\cos\theta_D\ \cos\theta_A)^2 \quad (1\text{-}4)$$

Where θ_T is the angle between the donor emission transition moment and the acceptor absorption transition moment, and θ_D and θ_A are the angles between the donor–acceptor connection line and the donor emission and the acceptor absorption transition moments, respectively.

The range of the Kappa square value is between 0 and 4. Given that both probes can undergo unrestricted isotropic motion, the Kappa square assumes a numerical value of 2/3.

- **The overlap integral**

The overlap integral is used to express the degree of overlap between the donor fluorescence spectrum and the acceptor absorption spectrum.

The overlap integral J is given by:

$$J = \int_0^\infty f_D(\lambda)\varepsilon_A(\lambda)\lambda^4 d\lambda \quad (1\text{-}5)$$

Where λ is the wavelength of the light, $\varepsilon A(\lambda)$ is the molar extinction coefficient of the acceptor at wavelength λ, and $f_D(\lambda)$ is the fluorescence spectrum of the donor normalized on the wavelength scale.

- **FRET efficiency**

The FRET efficiency (E) is the quantum yield of the energy transfer, which is the fraction of photons absorbed by the donor that are transferred to the receptor, defined as follows:

$$E = N_1 / N_2 \quad (1\text{-}6)$$

Where N_1 is the number of quanta transferred from the donor to the acceptor and N_2 is number of quanta absorbed by the donor.

E is dependent on the donor-to-acceptor separation distance (r) with an inverse 6th law as shown by the equation:

$$E = R_0^6 / (R_0^6 + r^6) \quad (1\text{-}7)$$

All in all, to achieve the FRET response in analytical detection, there are two factors are necessary: a donor–acceptor pair and an instrument to measure fluorescence. For selection of the donor–acceptor pair, these basic requirements should be considered:

- The alignment of the absorption and emission moments should be appropriate.
- The donor molecule must have a high quantum yield.
- The overlap of the emission spectrum of the donor molecule and the absorption spectrum of the acceptor molecule should be considerable.

Notably, the acceptor probe can be fluorescent or non-fluorescent.

1.1.2 FRET application

FRET has been widely used in the detection of both intramolecular and intermolecular interactions as well as in the detection of specific biomolecules using biosensors based on the FRET response [5-7]. Since fluorescence detection is very sensitive, it has been widely used in enzyme linked immunosorbent assays (ELISA), fluorescence polarization immunoassays, and genetic analysis by fluorescence in situ hybridization (FISH). Besides, FRET is a powerful spectroscopic and photophysical reporting technique. Acting as a "spectroscopic ruler", FRET-based techniques can be used to measure small changes (0.5–10 nm) in the distance between the donor and the acceptor, which can be used to measure *in vivo* protein–protein interaction. Additionally, the FRET response between two chromosomes can be used for detection of DNA protein interaction, nucleic acid hybridization, and DNA interaction with drugs, for examination of the primary and secondary structure of DNA fragments, and for DNA sequencing [7-11].

Therefore, the wide range of applications in many areas of environmental monitoring, clinical chemistry and genetic research makes FRET very important to analytical chemistry.

1.2 Quantum dots (QDs)

Quantum dots (QDs) are inorganic semiconductor nanocrystals, a cluster of thousands of atoms, whose size typically ranges from 1 to 20 nm [12]. QDs exhibit several unique photophysical properties, such as broad absorption spectra, narrow size-controlled fluorescence emission, high fluorescence quantum yield, and strong stability against photo-bleaching. The absorption spectra of QDs are broad, generally extending from the visible region to the ultraviolet. In comparison, QDs exhibit narrow emission spectra, usually within 50 nm. Both absorption and emission spectra scale with the size of the QDs [13]. For instance, the alteration of the CdSe cluster diameter from 200 to 20 Å can lead to the change of emission spectra from deep red to green [14]. In the near-infrared wavelength, the quantum yield ($\boldsymbol{\Phi}$) of quantum dots ($\boldsymbol{\Phi}$ around 0.2–0.7) is higher than that of the typical organic dye (0.05–0.25) [15]. With the development of stable synthesis techniques, the production of narrow size distribution of QDs has been accomplished. In addition, effective approaches have been developed to enable modification of QDs by various functional ligands. All of these properties allow QDs to be used in the development of a variety of biosensors, including QD-FRET sensors, QD-quenching sensors, QD-labeled intracellular imaging probes, and other format sensors.

1.2.1 CdSe QDs as FRET donors

Recently, QDs have been widely used for detection of nucleic acids and proteins [16]. The development of QDs provides suitable labels as the core of

fluorescence-based bioanalysis. In a number of studies, CdSe QD serves as one of the most popular energy donors. The CdSe QDs have several advantages, such as single-step synthesis, water solubility, relatively high fluorescence quantum yield (~46%), and narrow size distribution [17, 18]. The typical core-shell QD (CdSe-ZnS) is CdSe as a core with a ZnS shell. The ZnS shell protects the CdSe core from oxidation and prevents leaching of CdSe into the buffer solution, resulting in improvement of stability and photoluminescence yield of the CdSe core [13, 19]. The thickness of the ZnS shell can be chosen for different purposes. The thinner ZnS shells (1–2 monolayers) produce high photoluminescence yield, whereas the thicker ZnS shells (4–6 monolayers) can provide better protection of the CdSe core against extreme buffer conditions. Another reason why CdSe-ZnS is more popular than other QDs in analytical applications is that the size of core-shell nanocrystals can easily increase by a factor of two for red-emitting QDs compared to their blue-emitting counterparts [20].

Even though QDs have already been applied widely as FRET donors, the limitations of QDs still need to be improved. One limitation is that the size of QDs is larger than molecular dyes, which prevents the energy acceptors approaching close enough to donors. In most analytical applications, to enhance the analysis specificity QDs are functionalized on the surface according to specific requirements, which both enlarges QD sizes and improve analysis specificity, thus producing a complicated dilemma [21]. However, the size limitation of QDs can be taken used of. The large surfaces of colloidal QDs provide multi-reactive binding sites, and energy transfer to several FRET

acceptors can be realized. In this FRET system, QDs provide nanoscale scaffolds and act as central energy donors to the surrounding proximal acceptors by arraying a couple of copies of energy acceptors. The FRET cross-section is increased proportionally, resulting enhanced overall energy transfer efficiency [22]. For multi-acceptor-to-donor (QD) format, the overall energy transfer efficiency can be expressed as:

$$E(n, r) = n R_0^6 / (n R_0^6 + r^6) \quad (1\text{-}8)$$

where n is the number of total acceptors having energy transfer with the same donor, supposing that r is a fixed donor–acceptor distance. R_0 is the Förster distance of the pair of donor and acceptor [5, 7].

The enhancement in FRET efficiency in multi-acceptor-to-donor (QD) format has been demonstrated by numerous analytical studies of proteins with QD dye pairs compared with one-to-one donor acceptor format [5, 23]. In some FRET schemes, QDs serve as energy donors for the analysis of biomolecules and other small chemical molecules. Due to a number of unique optical properties, QDs are advantageous in the development of bioanalysis, especially based on FRET. For instance, superior brightness and resistance to photobleaching provide greater optimization of applications of QDs in FRET systems [21, 24-29]. Bioanalyses have been developed wherein QDs play an active role as energy donors in FRET. A number of well-known bioanalysis formats are based on QDs involved FRET, for example, molecular beacons [30-34], Taqman probes [30, 33], scorpion primers [33-35], and immunoassays [36, 37].

1.2.2 Selection of donor and acceptor pair

To achieve ultrasensitive detection using a FRET-based sensor, three main factors should be considered for the selection of the donor–acceptor pair and sensor configuration design. Increase of transfer energy efficiency should be considered first. According to Equation 1-8, with the fixed $\boldsymbol{R_0}$ and $\boldsymbol{r}$ of a given donor and acceptor pair, enhancement of FRET efficiency could be achieved by increasing the value of $\boldsymbol{n}$. Additionally, increasing the number of energy acceptors ($\boldsymbol{n}$) can also broaden the FRET dynamic range [5]. The second factor is reduction of the direct excitation of acceptors. Due to the broad absorption spectra of acceptors (e.g., conventional organic dye), the direct excitation contribution could adversely affect the final FRET response with decrease of the signal-to-noise ratio. In order to measure the FRET signal of the target more accurately, the excitation wavelength should be selected from within the absorption spectra of QD but far from the acceptor's absorption valley [5, 38]. The third consideration is that transfer efficiency strongly depends on the distance between the selected donor and acceptor ($\boldsymbol{r}$) and the Förster distance ($\boldsymbol{R_0}$), according to Equation 1-3. The Förster distance ($\boldsymbol{R_0}$) is determined by the given donor and acceptor. The distance between donor and acceptor ($\boldsymbol{r}$) depends on the design of FRET-based sensor configuration.

For example, the selection of QD 605 and Cy5 as a donor and acceptor pair, which is popular in the development of FRET-based nanosensor, has been widely used in many studies in biology and analytical chemistry [39-41]. The normalized absorption and emission spectra of QD 605 and Cy5 are shown in

Figure 1.3. Apart from the unique optical properties of QDs, there are other advantages such as the negligible crosstalk between the donor and acceptor, the excitation wavelength that could be chosen near the minimum of the Cy5 absorption spectrum, the large difference between the diameters of the donor and acceptor that allows several acceptors linked to one QD donor to enhance the FRET efficiency.

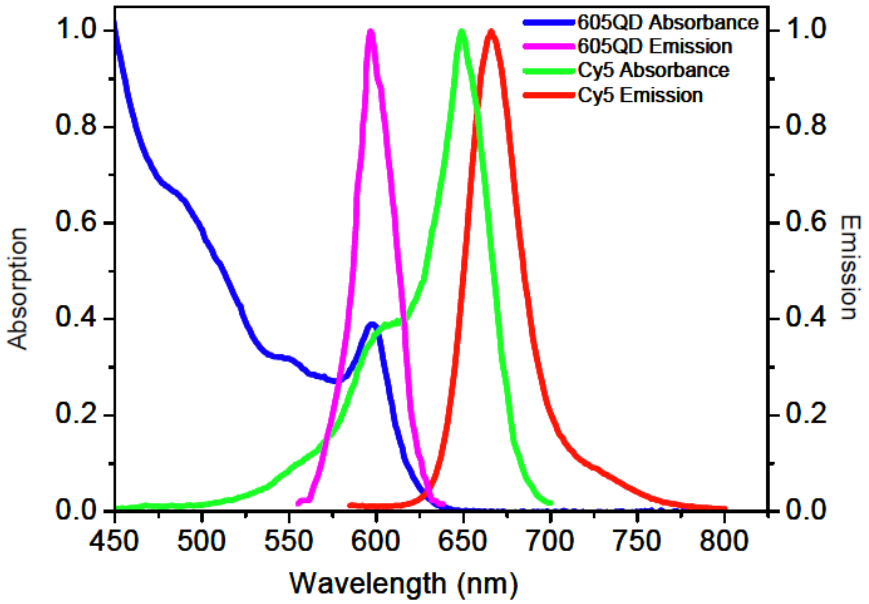

Figure 1.3 The normalized absorption and emission spectra of QD 605 and Cy5 [42]

1.2.3 Application of QD-based FRET

QDs are well established as labels for fluorescence imaging assays due to their optimal spectroscopic features and photochemical instability which can be applied to biological systems. With their unique photophysical properties, QDs are very popular for bioanalytical applications that can achieve the potential for spectral multiplexing without signal amplification being necessary. Besides, QDs could be attractive in near infrared fluorescence imaging *in vivo*. Moreover, QDs also have a potential future application for the combination of two or more biomedical imaging modules [7].

Aside from their unique potential, the properties of high fluorescence quantum yield and stability allows QDs to act as the donor in FRET systems for detection of biomolecules both *in vitro* and *in vivo*. Recent FRET investigations with QD as the energy donor indicate that these advantages, compared to conventional dyes, allows increased rates of FRET measurement and improvement of the signal-to-noise ratio. The significance of using QDs in a FRET detection system is that QD-protein conjugates (called nanoscale GPS) to derive protein conformation can be used to infer protein structure and further functionality studies [43]. A QD donor-based FRET system can be used to control the FRET rate and QD emission, which serves as a photochromic switch [5]. A QD-dye pair can also be constructed as a biomolecule sensor for specific detection, for example, for nutrient sugar maltose or explosive TNT [6, 44]. The QD conjugated probe can be used to monitor DNA replication *in vitro* based on FRET response [45]. A QD donor can also be applied to photodynamic medical

therapy [46], monitoring protein assembly [47, 48] and protein interaction near cellular membranes [47].

1.3 Binding-induced DNA assembly (BINDA)

DNA self-assembly is the spontaneous association of DNA, and is a common strategy for generating nanostructures based on noncovalent interactions [49, 50]. Unlike DNA self-assembly, recent studies show that binding-induced DNA assembly (BINDA) depends on the binding of two DNA-labeled affinity ligands to a single target molecule, returning in increase in the local effective concentration of complementary sequences [51-55]. Distinguished from DNA self-assembly, the formation of BINDA cannot take place until a specific target triggers a binding activity [56].

1.3.1 Principle of BINDA

The basic principle of BINDA can be briefly explained with the following scheme (Figure 1.4).

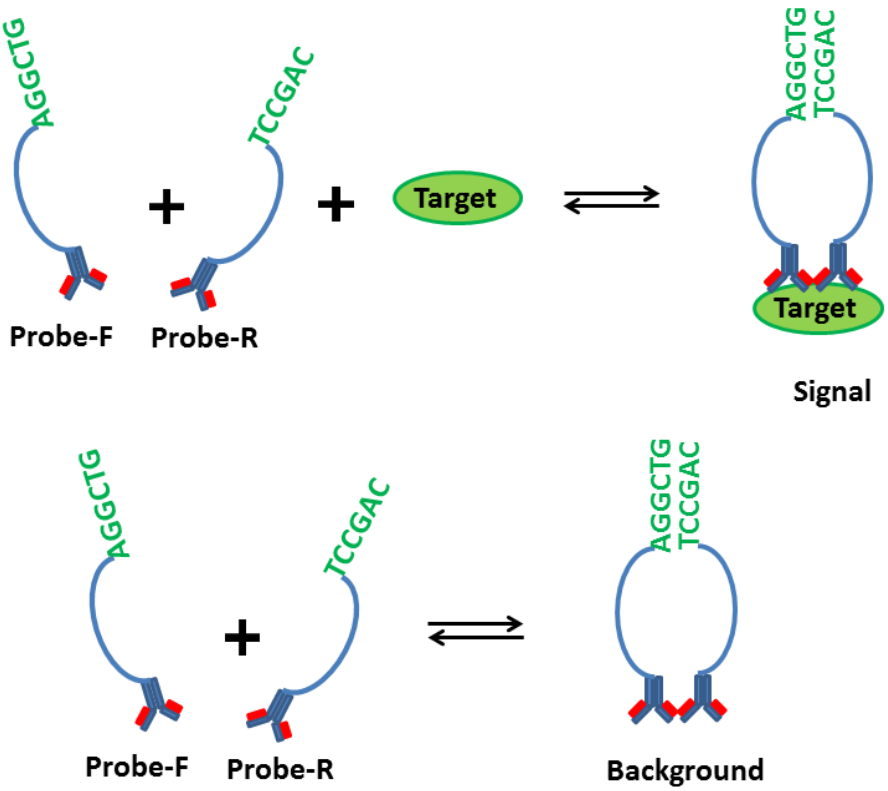

Figure 1.4 Schematic showing binding-induced DNA assembly that produces signal (top) and the target-independent assembly that produces background (bottom).

The essential principle of BINDA is that the nonspecific DNA self-assembly is difficult to achieve at low concentration, unless the effective local concentration of complementary sequences has been increased to the level which favors the hybridization of DNA sequences [55-59]. According to Figure 1.4, two affinity probes are first constructed by conjugating a DNA sequence to each affinity ligand. The green portions of the two DNA sequences are complementary. The two complementary sequences are so short that they cannot hybridize each other spontaneously. Binding to the single target molecule, the two probes hybridize each other on the complementary parts. The main reason that binding activity can induce DNA assembly is that binding to a single target molecule can greatly improve the local effective concentration of complementary sequences [60]. For example, when the concentration of DNA sequences is 1 nM, the distance between two complementary DNA strands is about 740 nm on average; but the distance between two complementary DNA strands can be shortened resulting from binding activity (~10 nm). If the distance is 10 nm, the local effective concentration of DNA strands could be around 40 μM. Due to binding activity, the dramatic increase in the local effective concentration of DNA greatly improves the melting temperature of complementary sequences, enabling binding-induced DNA assembly [56, 61-63].

The difference in melting temperature before and after binding-induced DNA assembly can be estimated. As shown in Figure 1.4, if two complementary sequences are present in two separate DNA stands, their melting temperature is lower than 10 °C. Therefore, the hybridization of these two complementary

sequences cannot happen at room temperature. If these two complementary sequences are placed into a limited local area triggered by a binding event, the melting temperature can be increased and the two complementary sequences can hybridize with each other. Correspondingly, the two complementary sequences in free probes cannot hybridize with each other because of the low melting temperature (10 °C).

1.3.2 Unique properties of BINDA:

BINDA has four main properties:

- Simultaneous binding of two ligands to a **single** target molecule.
- Homogeneous assembly of two DNA probes **without separation**.
- Conversion of **various** target-affinity ligands binding into DNA assembly.
- **Large range of applications** using the BINDA platform by changing the corresponding affinity ligands.

1.4 Aptamers

Aptamers are short DNA or RNA oligonucleotides that bind to target molecules with high affinity and specificity. Aptamers show great potential in the detection of biomolecules [61, 63-65]. Starting in 1990, RNA sequences that could bind to target molecules with high specificity were selected, isolated, and amplified by two groups independently [61, 62].

1.4.1 SELEX for selection of aptamers

The **S**ystematic **E**volution of **L**igands by **EX**ponential enrichment (**SELEX**) process is a method that allows nucleic acids generated from enormous libraries to recognize target molecules with high affinity and specificity *in vitro* [50, 61, 62, 66, 67]. The SELEX method involves four steps: library generation, partition, elution, and amplification. The initial nucleic acid library is synthesized with a randomized segment in the middle section of its sequence [61, 62]. In the first step, incubation of the initial nucleic acid library with the target molecule can generate specific complexes under certain conditions. The second step is partition of unbound nucleic acids from the nucleic acid library. The final step is the amplification of successful nucleic acids to obtain an enriched pool of aptamers after evolution.

To improve the performance of the SELEX process, many advanced SELEX methods have been developed based on the original SELEX. The cDNA-SELEX replaces classical techniques with synthetic pools, *in vivo* SELEX is the first attempt to enter the cell environment, and so on [68]. Among the four steps in SELEX, the partition should be the most important step. Therefore, many modern techniques updated the SELEX method by improving the partition process. For example, capillary electrophoresis selection (CE-SELEX) is used for the separation of aptamer–target complexes by differential electrophoretic migration due to the difference in size between the free target and the aptamer–target complexes [69]. The MonoLEX is named because high affinity sequences can be selected in a single cycle [70]. In MonoLEX selection, chromatography

and vigorous column washing play a central role. Microfluidics SELEX (M-SELEX) is an approach as a single step of SELEX including sample incubation and transportation, aptamer screening and fast amplification on microfluidics chips with minuscule channels [71].

For specific objectives, the basic SELEX method has been developed in many different ways. The target expressed on cell surface SELEX (TECS-SELEX) is a typical new approach of SELEX which is used for target proteins on the cell surface with a system of ectopic expression. In contrast to TECS-SELEX, without the system of ectopic expression, the cell specific SELEX (CS-SELEX) is utilized to select aptamers against cancer-specific cell markers in T-cell acute lymphoblastic leukemia cell line.

1.4.2 Advantages of aptamers

Aptamers have many advantages over antibodies. Firstly, RNA aptamers form unique secondary or tertiary structures with high specificity to their target molecules, even the small molecules, such as the hydroxyl group. Secondly, aptamers can be generated for any protein through the SELEX procedure. In addition, the SELEX process is *in vitro*, avoiding the immune response of generation of antibodis. Thirdly, the selection of aptamers can be optimized under any conditions, whereas the selection of antibodies can only work under physiological conditions. Aptamers are more stable than antibodies at high temperatures. Finally, aptamer can be regenerated easily after denaturation. The

chemical synthetic process of aptamer allows the quality of aptamer to be more consistent than that of antibodies.

1.4.3 Aptamer-based biosensors

Compared to using natural receptors (antibodies and enzymes), aptamer-based biosensors have become increasingly important molecular tools. There are three main advantages for aptamer-based biosensors. Firstly, the high reproducibility and purity of synthesis using commercial technologies lead to high chemical stability of DNA aptamers compared with antibodies and enzymes. Secondly, the selection process is more efficient and effective *in vitro*. In principle, SELEX can be used for any given target, for example, small molecules, large proteins, and cells, which ensures that aptamer-based biosensors can potentially be used for a wide range of targets. Thirdly, the flexibility of design of aptamer-based biosensors depends on the given target, achieving high sensitivity and selectivity of detection [72-74].

For the design of aptamer-based biosensors, there are two major categories of assay configuration: single-site binding and dual-site binding based on different recognition sites between the aptamer and target [65]. For single-site binding, the aptamer could serve as a pocket to trap the target molecule (for small molecules only), or serve as an affinity ligand binding to the surface of target (both for small molecules and macromolecules). Both single-site and dual-site binding modes rely on the availability of the aptamer-target pair. In addition, for dual-site binding, two aptamers should bind to different regions of the target [75].

In the last 10 years, QD-aptamer fluorimetric biosensors have played a significant role for detection of different targets with several assay formats. In a homogeneous manner, the QD-aptamer fluorimetric biosensors can generate unique short-range interaction readout mechanism and ratio metric. Although few QD-aptamer fluorimetric biosensors have been used for real clinical samples, the attempt to design biosensors still is still attractive to scientists. The outlook of development of QD-aptamer fluorimetric biosensors will focus on improvement of sensitivity, specificity, and stability in order to extend their application in real clinical science and basic biological research.

1.5 Platelet-Derived Growth Factor (PDGF)

PDGF is a kind of dimeric glycoprotein. After the first identification of platelet derived growth factor (PDGF) by Ross and co-workers in 1974, PDGFs have been shown to play an important role in proliferation, survival, migration, and deposition of extracellular matrix (ECM).

1.5.1 Different isomers of PDGF

In 1986, Heldin et al. demonstrated that PDGF-AA is the osteosarcoma cell-derived growth factor (ODGF) reported in 1980. Subsequent analysis of PDGF showed a mixture of 70% PDGF-AB and 30% PDGF-BB from human platelets by Hammacher et al. in 1988. In 1990, Hart et al. reported that PDGF-AA also existed in human platelets. Additionally, the isomers PDGF-AA/-AB/-BB bind to different PDGF receptor specifically. Platelet derived growth factor

receptor (PDGFR) is classified as a receptor tyrosine kinase (RTK), a type of cell surface receptor. PDGFRs also function as homo- and heterodimers for PDGF-AA, PDGF-BB, and PDGF-AB with different affinities [76-78]. PDGF-AB could stimulate chemotaxis and actin reorganization to form circular membrane ruffles. However, PDGF-AA and PDGF-BB revealed difference. Both isomers stimulated mitogenicity in human foreskin fibroblasts, albeit with low potency in the case of PDGF-AA.

1.5.2 PDGF and disease

A number of human diseases have been associated with the abnormal PDGF or PDGFR expression or activity in human patients. PDGFs contribute to neural development, vascular and hematopoietic development, neural crest cell development, organogenesis, somitogenesis and skeletal patterning [79]. The PDGFB and PDGFRβ play an essential role in development of cells in the vasculature. The PDGFA and PDGFα are important for neural crest and organ development. PDGFs have been implicated in the etiology of human cancer in which hyperactivity of PDGF has been observed. For example, in a mouse model, the formation of oligodendrogliomas is induced by the overexpression of PDGFB. PDGF also cooperated with Ink4a-Arf, a kind of tumor suppressor gene, which is involved in the malignant progression of gliomas. Besides, the concentration of PDGFs influences the express level of PDGFRs. Furthermore, in the progression of human cancer, PDGFs and PDGFRs interact with other oncogenes or tumor suppressor genes. Although how PDGFs and PDGFRs are regulated at the level of

transcription and maturation is not yet fully understood, the ultrasensitive detection of PDGFs concentration is useful for monitoring diseases. To address these clinical problems effectively, we need to detect the concentration of PDGF and understand the specific cellular functions that are affected by concentration of PDGF in physiology.

1.5.3 Biosensor for detection of PDGFs

The aptamer-based biosensor can be designed to be able to separate protein isomers of PDGF. PDGF-AB is a heterodimer, consisting of an A-chain and B-chain, while PDGF-BB is a homodimer, consisting of two B-chains. Aptamers against PDGF isomers bind only to the B-chain but not to the A-chain. For example, when the biosensor design is based on the interaction between the aptamer for B-chain and B-chain on PDGF, the method can discriminate PDGF-BB from PDGF-AB and PDGF-AA.

1.6 Thesis Objectives

This research aims to develop a binding-induced DNA nanosensor based on FRET. Applications of the DNA nanosensor include a homogeneous assay for the detection of nucleic acids and proteins.

Highly sensitive and specific detection of biomolecules, especially proteins and nucleic acids, contributes to both fundamental biological research and clinical diagnostics. Homogeneous binding assays can be performed in a single tube without any separation or washing steps, achieving fast detection in a

simple process. Because homogeneous assays eliminate the separation and washing procedures, the requirements for target recognition and signal transduction are more stringent. To meet these requirements, we have developed a binding-induced DNA assembly (BINDA) strategy. This DNA assembly is triggered by a binding event and can be detected using many signal transduction techniques. The primary objective of this research is to develop a nanosensor that adapts the principle of binding-induced DNA assembly and that takes advantage of the fluorescence properties of quantum dots (QDs). Without the need for separation or enzymatic amplification, this nanosensor can be applied to assays for biomolecules through the monitoring of fluorescence resonance energy transfer (FRET), with high sensitivity and specificity.

I describe a binding-induced DNA nanosensor and its application to homogenous detection of DNA and proteins. This nanosensor was based on the binding-induced assembly of fluorescently labeled DNA on DNA-functionalized quantum dots, resulting in FRET between the quantum dots (QD 605) and the fluorescent dye (Cy5). The sensor was applied to the detection of a single-nucleotide polymorphism (SNP) in the *p53* gene sequence and the detection of PDGF, with pM detection limits. This strategy can be applied to develop assays for a wide range of targets by functionalizing the surface of quantum dots with appropriate affinity ligands (e.g., aptamers and antibodies).

This project had three objectives:

i. To develop and optimize a DNA nanosensor based on binding-induced FRET for the detection of model DNA target;

ii. To utilize the DNA nanosensor for the detection of a mutated DNA fragment from the *p53* gene.

iii. To utilize the DNA nanosensor for the sensitive and specific detection of PDGF-BB.

The development and optimization of the DNA nanosensor based on binding-induced FRET is thoroughly discussed in Chapter 2. The optimized method was then used for the detection of the model DNA target. In order to evaluate the usefulness of the DNA nanosensor, the method was used for DNA and protein detection. Chapter 3 assesses the ability of the DNA nanosensor to detect a *p53* gene point mutation. Chapter 4 describes the detection of PDGF-BB, an example of a protein target. Chapter 5 discusses the final conclusions of this project.

1.7 References

1. Weber, G. *Adv. Protein Chem.* **1953,** *8,* 415-459.

2. Clapp, A. R.; Medintz, I. L.; Uyeda, H. T.; Fisher, B. R.; Goldman, E. R.; Bawendi, M. G.; Mattoussi, H. *J. Am. Chem. Soc.* **2005,** *127,* 18212-18221.

3. Gordon, G. W.; Berry, G.; Liang, X. H.; Levine, B.; Herman, B. et al. *Biophys. J.* **1998,** *74,* 2702-2713.

4. Bernard, V. Molecular Fluorescence: Principles and Applications; Wiley-VCH, **2001.** 48.

5. Clapp, A. R.;Medintz, I. L.; Mauro, J. M.; Fisher, B. R.; Bawendi, M. G.; Mattoussi, H. J. *Am. Chem. Soc.* **2004,** *126,* 301-310.

6. Medintz, I. L.; Clapp, A. R.; Mattoussi, H.; Goldman, E. R.; Fisher, B.; Mauro, J. M. *Nat. Mater.* **2003,** *2,* 630-638.

7. Lakowicz, J.R. Principles of Fluorescence Spectroscopy; Springer Science and Business Media: New York, 2006.

8. Miyawaki, A. *Dev. Cell* **2003,** *4,* 295-305.

9. Jares-Erijman, E. A.; Jovin, T. M. *Nat. Biotechnol.* **2003,** *21,* 1387-1395.

10. Wu, P. G.; Brand, L. *Anal. Biochem.* **1994,** *218,* 1-13.

11. Didenko, V.V. *BioTechniques* **2001,** *31,* 1106.

12. Alivisatos, A.P. *Science (Washington, DC)* **1996,** *271,* 933-937.

13. Dabbousi, B. O.; RodriguezViejo, J.; Mikulec, F. V.; Heine, J. R.; Mattoussi, H.; Ober, R.; Jensen, K. F.; Bawendi, M. G. *J. Phys. Chem. B,* **1997,** *101,* 9463-9475.

14. Murray, C. B.; Norris, D. J.; Bawendi, M. G. *J. Am. Chem. Soc.* **1993,** *115,* 8706-8715.

15. Resch-Genger, U.; Grabolle, M.; Cavaliere-Jaricot, S.; Nitschke, R.; Nann, T. *Nat. Methods* **2008,** *5,* 763-775.

16. Sapsford, K. E.; Pons, T.; Medintz, I. L.; Mattoussi, H. *Sensors* **2006,** *6,* 925-953.

17. Baumle, M.; Stamou, D.; Segura, J. M.; Hovius, R.; Vogel, H. *Langmuir* **2004,** *20,* 3828-3831.

18. Palaniappan, K.; Xue, C. H.; Arumugam, G.; Hackney, S. A.; Liu, *J. Chem. Mater.* **2006,** *18,* 1275-1280.

19. Hines, M. A.; Guyot-Sionnest, P. *J. Phys. Chem.* **1996,** *100,* 468-471.

20. Mattoussi, H.; Cumming, A. W.; Murray, C. B.; Bawendi, M. G.; Ober, R. *Phys. Rev. B: Condens. Matter* **1998,** *58,* 7850-7863.

21. Medintz, I. L.; Uyeda, H. T.; Goldman, E. R.; Mattoussi, H. *Nat. Mater.* **2005,** *4,* 435-446.

22. Sapsford, K. E.; Pons, T.; Medintz, I. L.; Higashiya, S.; Brunel, F. M.; Dawson, P. E.; Mattoussi, H. *J. Phys. Chem. C* **2007,** *111,* 11528-11538.

23. Clapp, A. R.; Medintz, I. L.; Mattoussi, H. *Chemphyschem* **2006,** *7,* 47-57.

24. Bruchez, M.; Moronne, M.; Gin, P.; Weiss, S.; Alivisatos, A. P. *Science (Washington, DC)* **1998,** *281,* 2013-2016.

25. Chan, W. C. W.; Nie, S. M. *Science (Washington, DC)* **1998,** *281,* 2016-2018.

26. Gao, X. H.; Yang, L. L.; Petros, J. A.; Marshal, F. F.; Simons, J. W.; Nie, S. M. *Curr. Opin. Biotechnol.* **2005,** *16,* 63-72.

27. Parak, W. J.; Pellegrino, T.; Plank, C. *J. Nanosci. Nanotechnol.* **2005,** *16,* 9-25.

28. Pinaud, F.; Michalet, X.; Bentolila, L. A.; Tsay, J. M.; Doose, S.; Li, J. J.; Iyer, G.; Weiss, S. *Biomaterials* **2006,** *27,* 1679-1687.

29. Smith, A. M.; Gao, X. H.; Nie, S. M. *J. Photochem. Photobiol.* **2004,** *80,* 377-385.

30. Epstein, J. R.; Biran, I.; Walt, D. R. *Anal. Chim. Acta* **2002,** *469,* 33-36.

31. Yang, C. Y. J.; Medley, C. D.; Tan, W. H. *Curr. Pharm. Biotechnol.* **2005,** *6,* 445-452.

32. Tan, W. H.; Wang, K. M.; Drake, T. *J. Curr. Opin. Chem. Biol.* **2004,** *8,* 547-553.

33. Ranasinghe, R. T.; Brown, T. *J. Chem. Soc., Chem. Commun.* **2005,** *44,* 5487-5502.

34. Marras, S. A. E.; Tyagi, S.; Kramer, F. R. *Clin. Chim. Acta* **2006,** *363,* 48-60.

35. Solinas, A.; Brown, L. J.; McKeen, C.; Mellor, J. M.; Nicol, J. T. G.; Thelwell, N.; Brown, T. *Nucleic Acids Res.* **2001,** *29,* e96.

36. Ohiro, Y.; Arai, R.; Ueda, H.; Nagamune, T. *Anal. Chem.* **2002,** *74,* 5786-5792.

37. Pulli, T.; Hoyhtya, M.; Soderlund, H.; Takkinen, K. *Anal. Chem.* **2005,** *77,* 2637-2642.

38. Medintz, I. L.; Clapp, A. R.; Brunel, F. M.; Tiefenbrunn, T.; Uyeda, H. T.; Chang, E. L.; Deschamps, J. R.; Dawson, P. E.; Mattoussi, H. *Nat. Mater.* **2006,** *5,* 581-589.

39. Zhang, Y.; Zhang, C. Y. *Anal. Chem.* **2012,** *84*, 224-231.

40. Wu, Y.; Ho, Y. P.; Mao, Y. C.; Wang, X. M.; Yu, B.; Leong, K. W.; Lee, L. J. *Mol. Pharm.* **2011,** *8,* 1662-1668.

41. Kawashima, N.; Nakayama, K.; Itoh, K.; Itoh, T.; Ishikawa, M.; Biju, V. *Chem.--Eur. J.* **2010,** *16,* 1186-1192.

42. Zhang, C. Y.; Yeh, H. C.; Kuroki, M. T.; Wang, T. H. *Nat. Mater.* **2005,** *4,* 826-831.

43. Medintz, I. L.; Konnert, J. H.; Clapp, A. R.; Stanish, I.; Twigg, M. E.; Mattoussi, H.; Mauro, J. M.; Deschamps, *J. R. Proc. Natl. Acad. Sci. U. S. A.* **2004,** *101,* 9612-9617.

44. Goldman, E. R.; Medintz, I. L.; Whitley, J. L.; Hayhurst, A.; Clapp, A. R.; Uyeda, H. T.; Deschamps, J. R.; Lassman, M. E.; Mattoussi, H. *J. Am. Chem. Soc.* **2005,** *127,* 6744-6751.

45. Patolsky, F.; Gill, R.; Weizmann, Y.; Mokari, T.; Banin, U.; Willner, I. *J. Am. Chem. Soc.* **2003,** *125,* 13918-13919.

46. Samia, A. C. S.; Chen, X. B.; Burda, C. *J. Am. Chem. Soc.* 2003. **2003,** *125,* 15736-15737.

47. Kloepfer, J. A.; Cohen, N.; Nadeau, J. L. *J. Phys. Chem. B* **2004,** *108,* 17042-17049.

48. Sapsford, K. E.; Medintz, I. L.; Golden, J. P.; Deschamps, J. R.; Uyeda, H. T.; Mattoussi, H. *Langmuir* **2004,** *20,* 7720-7728.

49. Whitesides, G. M.; Boncheva, M. *Proc. Natl. Acad. Sci. U. S. A.* **2002,** *99,* 4769-4774.

50. Lehn, J.M. *Chem. Scr.* **1988,** *28,* 237-262.

51. Fredriksson, S.; Gullberg, M.; Jarvius, J.; Olsson, C.; Pietras, K.; Gustafsdottir, S. M.; Ostman, A.; Landegren, U. *Nat. Biotechnol.* **2002,** *20,* 473-477.

52. Soderberg, O.; Gullberg, M.; Jarvius, M.; Ridderstrale, K.; Leuchowius, K. J.; Jarvius, J.; Wester, K.; Hydbring, P.; Bahram, F.; Larsson, L. G.; Landegren, U. *Nat. Methods,* **2006,** *3,* 995-1000.

53. Schallmeiner, E.; Oksanen, E.; Ericsson, O.; Spangberg, L.; Eriksson, S.; Stenman, U. H.; Pettersson, K.; Landegren, U. *Nat. Methods,* **2007,** *4,* 135-137.

54. Heyduk, T. *Biophys. Chem.* **2010,** *151,* 91-5.

55. Gorin, D. J.; Kamlet, A. S.; Liu, D. R. *J. Am. Chem. Soc.* **2009,** *131,* 9189.

56. Heyduk, E.; Dummit, B.; Chang, Y. H.; Heyduk, T. *Anal. Chem.* **2008,** *80,* 5152-5159.

57. Li, F.; Zhang, H. Q.; Lai, C.; Li, X. F.; Le, X. C. *Angew. Chem., Int. Ed. Engl.* **2012,** *51,* 9317-9320.

58. Bini, A.; Minunni, M.; Tombelli, S.; Centi, S.; Mascini, M. *Anal. Chem.* **2007,** *79,* 3016-3019.

59. Di Giusto, D. A.; Wlassoff, W. A.; Gooding, J. J.; Messerle, B. A.; King, G. C. *Nucleic Acids Res.* **2005,** *33,* e64.

60. Heyduk, E.; Dummit, B.; Chang, Y. H.; Heyduk, T. *Anal. Chem.* **2008,** *80,* 5152-5159.

61. Tuerk, C. and Gold, L. *Science (Washington, DC)* **1990,** *249,* 505-510.

62. Ellington, A. D. and Szostak, J. W. *Nature* **1990,** *346,* 818-822.

63. Tombelli, S. and Minunni, M.; Mascini, M. *Biomol. Eng.* **2007,** *24,* 191-200.

64. Ellington, A. D. and Szostak, J. W. *Nature* **1992,** *355,* 850-852.

65. Hermann, T. and Patel, D. J. *Science (Washington, DC)* **2000,** *287,* 820-825.

66. Petach, H. and Gold, L. *Curr. Opin. Biotechnol.* **2002,** *13,* 309-314.

67. Kotia, R. B.; Li, L. J.; Mcgown, L. B. *Anal Chem.* **2000,** *72,* 827-831.

68. Chen, L.; Yun, S. W.; Seto, J.; Liu, W.; Toth, M. *Neuroscience (Oxford)* **2003,** *120,* 1005-1017.

69. Chen, F.; Hu, Y. L.; Li, D. Q.; Chen, H. D.; Zhang, X. L. *PLoS One.* **2009;** *4,* e8142.

70. Nitsche, A.; Kurth, A.; Dunkhorst, A.; Panke, O.; Sielaff, H.; Junge, W.; Muth, D.; Scheller, F.; Stocklein, W.; Dahmen, C.; Pauli, G.; Kage, A. *BMC Biotechnol.* **2007,** *7,* 48.

71. Mosing, R. K. and Bowser, M. T. *J. Sep. Sci.* **2007,** *30,* 1420-1426.

72. Clark, S. L. and Remcho, V. T. *Electrophoresis* **2002,** *23,* 1335-1340.

73. Willner, I. and Zayats, M. *Angew. Chem.* **2007,** *46,* 6408-6418.

74. Tombelli, S.; Minunni, M.; Mascini, M. *Biosens. Bioelectron.* **2005,** *20,* 2424-2434.

75. Song, S. P.; Wang, L. H.; Li, J.; Zhao, J. L.; Fan, C. H. *TrAC, Trends Anal. Chem.* **2008,** *27,* 108-117.

76. Heldin, C. H. and Westermark, B. *Physiol Rev.* **1999,** *79,* 1283-1316.

77. He, H.; Levitzki, A.; Zhu, H. J.; Walker, F.; Burgess, A.; Maruta, H. *J. Biol. Chem.* **2001,** *276,* 26741-26744.

78. Bergsten, E.; Uutela, M.; Li, X. R.; Pietras, K.; Ostman, A.; Heldin, C. H.; Alitalo, K.; Eriksson, U. *Nat. Cell Biol.* **2001,** *3,* 512-516.

79. Hoch, R. V. and Soriano, P. *Development.* **2003,** *130,* 4769-4784.

80. Huang, C. C.; Chiu, S. H.; Huang, Y. F.; Chang, H. T. *Anal. Chem.* **2007,** *79.* 4798-4804.

81. Huang, C. C.; Huang, Y. F.; Cao, Z. H.; Tan, W. H.; Chang, H. T. *Anal. Chem.* **2005,** *77,* 5735-5741.

82. Huang, C. C.; Chiang, C. K.; Lin, Z. H.; Lee, K. H.; Chang, H. T. *Anal. Chem.* **2008,** *80,* 1497-1504.

Chapter 2: Development of a DNA nanosensor based on binding-induced fluorescence resonance energy transfer

2.1 Introduction

My ultimate research goal is to develop homogeneous assays that can be useful for potential point-of-care applications and/or on-site analyses [1]. To achieve this goal, my first objective was to develop a fluorescence resonance transfer energy (FRET) assay format that could incorporate binding-induced DNA assembly (BINDA) [2].

In this chapter, I describe the strategy and the development of such an assay format, a nanosensor. The nanosensor is able to assemble the fluorescently labeled oligonucleotide onto the functionalized quantum dot (QD) [3], generating a binding-induced FRET signal for detection [4-7]. To optimize the nanosensor, I have studied a number of parameters, including the type and pH of reaction buffer, incubation time and temperature, selection of oligonucleotides for probes, surface coverage of QD, and the ratio of capture probe to adjunct probe to report probe.

2.2 Experimental methods

2.2.1 Reagents

The streptavidin-functionalized 605 QDs was purchased from Invitrogen (Carlsbad, CA). The oligonucleotides were all custom synthesized, labeled, and purified by Integrated DNA Technologies (Coralville, IA). Table 2.1 lists the

oligos used in Chapter 2. The oligos of the adjunct probe and capture probe are labeled to biotin groups at the 3' end. The oligo of report probe is modified with a Cy5 at the 5' end and biotin at the 3' end. The complementary sequences of the adjunct probe and report probe are highlighted in green in Table 2.1. The flexible linkers of adjunct probes are highlighted in blue. All solutions were prepared with phosphate buffered saline (1 × PBS) buffer (137 mM NaCl, 10 mM phosphate, 2.7 mM KCl, pH 7.4) that was diluted with deionized water from 10 × PBS buffer (Fisher Scientific, Nepean, ON). All other reagents were of analytical grade.

Table 2.1 DNA sequences used to construct the DNA nanosensor

DNA name			**Sequences**
Adjunct Probe	**Complementary sequences design**	**C1**	5'-**GTCCGTTTTTT**-Biotin -3'
		C2	5'-**GTC CG ATTTTT T**-Biotin -3'
		C3	5'-**TGTC CG ATTTTTT**-Biotin -3'
		C4	5'- **ATG TCC GATTTT TT**-Biotin -3'
	Flexible DNA linker design	**2T**	5'-**GTCCGTT**-Biotin-3'
		6T	5'- **GTCCGTTTTTT**-Biotin -3'
		10T	5'- **GTCCGTTTTTTTTTT**-Biotin -3'
		14T	5'- **GTCCGTTTTTTTTTTTTTT**-Biotin -3'
		18T	5'- **GTCCGTTTTTTTTTTTTTTTTTT**-Biotin -3'
Capture probe			5'- **TGT GAT TGC TGT GTG TTT TTT TTT TTT TTT TTT TT**-Biotin -3'
Report probe			5'-**Cy5**-**TCG GAC ATT ATT TTT TTT TTT TTT TTT TTT TTT TTT TGT AGG ACT GAG TTG G** -3'
Model DNA sequence			5'- **CAC ACA GCA ATC ACA TTC CAA CTC AGT CCT AC** -3'

2.2.2 Fluorescence Measurements

Fluorescence spectra were recorded by using a Photon Technology International MP1 fluorescence system. Fluorescence intensity was measured by using a DTX 880 multimode detector (Beckman Coulter Canada, Mississauga, ON) fluorescence plate reader. The 96-well black microplates (Corning, Lowell, MA) were used to load samples and 100 μL of sample solutions were added to each well. In order to quantify the difference in the FRET signal between sample and blank solutions, the fold change of the FERT response was used.

The FRET response is calculated by dividing the ratio of acceptor and donor emission intensities in the absence and presence of the target, respectively:

$$Fold\ Change = [(IS_{680} / IS_{605}) - (IB_{680} / IB_{605})] / (IB_{680} / IB_{605})$$

Where IS_{680} and IB_{680} are the fluorescence emission intensities at 680 nm in the presence and absence of target, respectively; and IS_{605} and IB_{605} are the fluorescence emission intensities at 605 nm in the presence and absence of target, respectively.

2.2.3 Functionalization of QDs

The biotinylated capture probe and adjunct probe were conjugated to streptavidin-coated QDs through the streptavidin and biotin interaction. Typically, the solution containing the desired concentration of biotinylated capture probe and biotinylated adjunct probe was mixed with streptavidin-coated QD solution. The mixture was then incubated at 37 °C for 30 min, and stored in a 4 °C fridge before use (Figure 2.1).

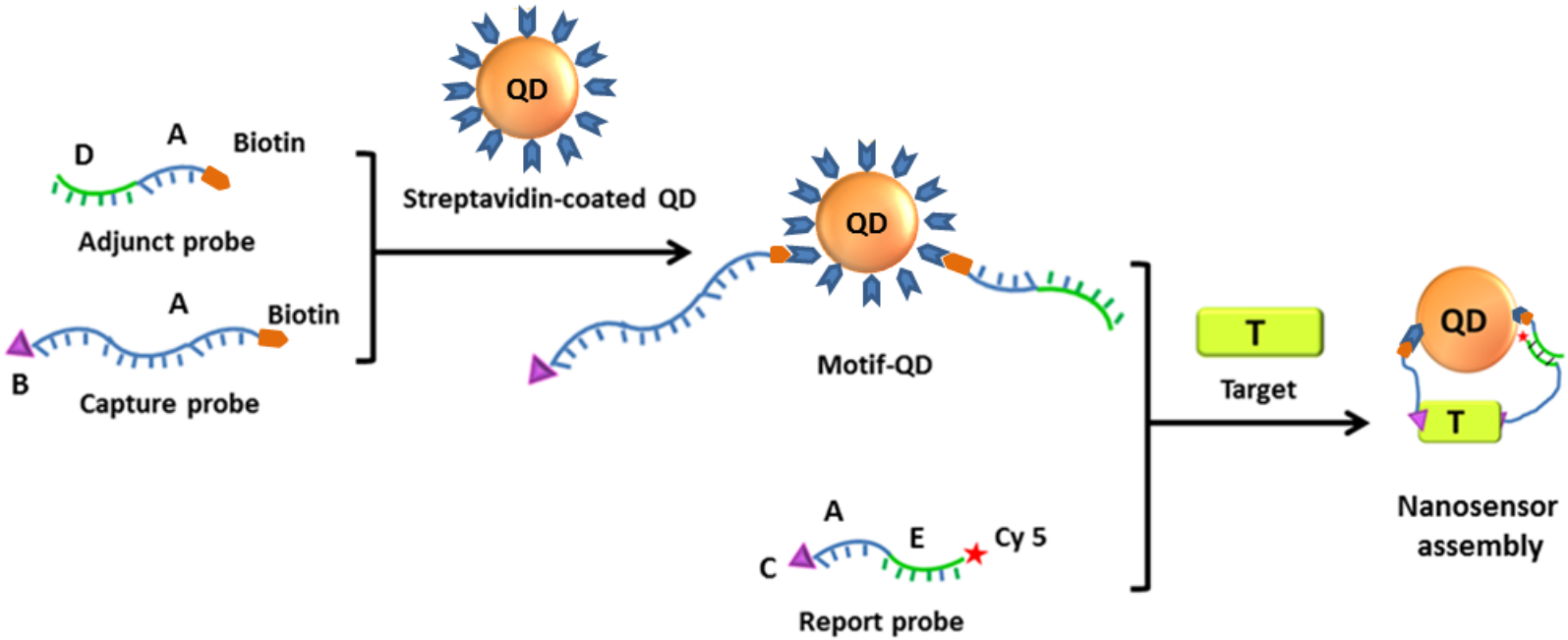

Figure 2.1 Schematic showing the construction of the binding-induced DNA nanosensor. A: flexible DNA linkers (blue); B and C: affinity ligands (purple); D and E: complementary oligonucleotides (green); T: the target molecule of interest.

2.2.4 Experimental optimization of the nanosensor using a model DNA target

To optimize the detection system, I first designed a DNA nanosensor for detection of a model DNA sequence by using complementary sequences to the model DNA sequence as the affinity ligands (Figure 2.2). The overall objective of optimization was to achieve the maximum difference in the FRET signal between sample and blank solutions. All triplicate sample and blank (without the model DNA target) solutions (100 μL) were prepared in 1 × phosphate buffered saline (PBS, pH 7.4). Each solution was incubated at 37 °C for 30 min and then at 25 °C for another 10 min before detection. One hundred microliters of each solution was then added to a 96-well microplate and detected by a multimode microplate reader (DTX 880 multimode detector) with excitation at 475 nm wavelength and emission at both 605 nm and 680 nm.

The optimization of the length and GC content of the complementary sequence on the adjunct probe was carried out by comparing the performances of different pairs of adjunct probe and report probe for analysis of 30 nM of model DNA target. Four different functionalized QD solutions (140 μL each) were prepared in 1 × PBS buffer. Each functionalized QD solution (10 nM) contained 150 nM adjunct probe (complementary sequences design—C1, C2, C3, C4), 150 nM capture probe, and 10 nM QD (Table 2.1) incubated at 37 °C for 30 min. In the next step, four sample solutions (100 μL) were prepared in 1 × PBS buffer with different functionalized QD solutions. Each final sample solution contained 1 nM functionalized QD solution, 30 nM report solution, and 30 nM model DNA target. Four corresponding blank solutions (100 μL) that contained all the reagents

but not the model DNA target were analyzed under the same conditions as for the detection of sample solutions, and the analyses of these blank solutions provided information on the magnitude of background. Sample and blank solutions were incubated at 37 ℃ for 30 min and then at 25 ℃ for another 10 min before detection. The difference in fold change of fluorescence response which involved both sample and blank solutions was used to evaluate the performance of four different kinds of adjunct probes.

To optimize the length of flexible DNA linker on the adjunct probe, five different functionalized QD solutions (140 μL) were prepared in 1 × PBS buffer with five different kinds of adjunct probe (flexible DNA linker design 2T, 6T, 10T, 14T, 18T) (150 nM), capture probe (150 nM), and 10 nM QD (Table 2.1) and were incubated at 37 ℃ for 30 min. The sample solutions (30 nM target) and blank solutions were prepared with 30 nM report probe.

To further improve the nanosensor performance, I optimized the ratio of adjunct probe to capture probe (capture probe only, 1:4, 1:2, 1:1, 2:1, 4:1, adjunct probe only) and the surface coverage on functionalized QD for analysis of model DNA sequences (10 nM).

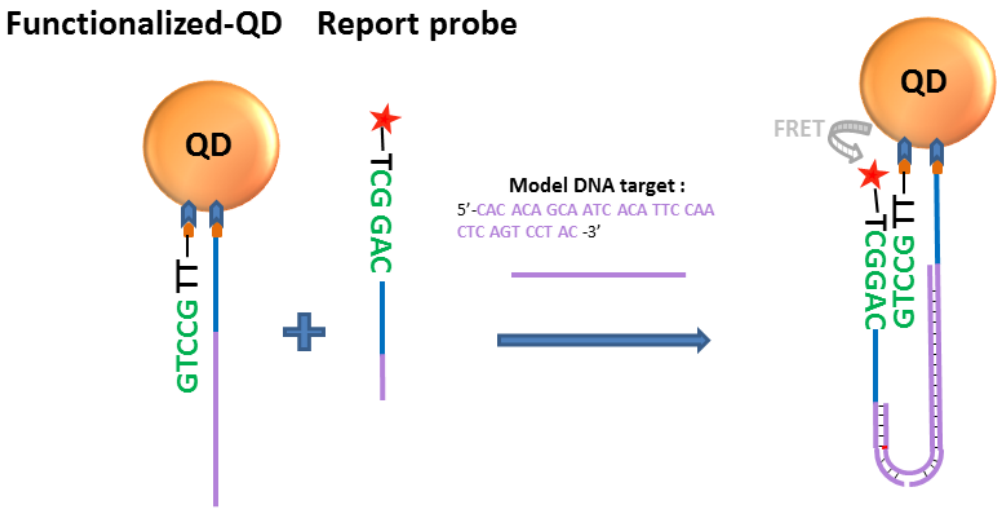

Figure 2.2 Schematic showing the construction of nanosensor for the detection of nucleic acids.

Affinity ligands (purple) functionalized capture probe and adjunct probe are each conjugated to the QD 605. Report probe is modified by Cy5 and another affinity ligand (purple) on each end. The binding of model DNA target with two DNA affinity ligands (the complementary sequences of model DNA target in the chapter) results in a stable binding-induced DNA assembly which generates the FRET signal.

2.3 Results and Discussion

2.3.1 Construction of the DNA nanosensor based on the binding-induced FRET

The key concept of the DNA nanosensor is using target binding to trigger the assembly between fluorescently-labeled DNA probes and the functionalized QDs, which otherwise cannot occur in the absence of target molecules. This assembly brings the FRET acceptor in the DNA probe and the QD serving as the donor into close proximity, generating a FRET signal. The intensity of the FRET signal is proportional to the concentration of target. Therefore, the measurement of FRET signal can be applied to quantification of the target.

The DNA nanosensor is constructed to comprise two key components, a functionalized QD and a report probe, as shown in Figure 2.1. The QD is conjugated to a number of adjunct probes and capture probes. The capture probe contains an affinity ligand to bind to the target molecule. The adjunct probe is a biotinylated oligonucleotide containing a short complementary sequence and a DNA flexible linker. The report probe is composed of a second affinity ligand and another complementary sequence. A fluorophore is labeled at the free end of this complementary sequence. The complementary sequences (5–8 n.t.) are so short that the duplex between them is not stable at room temperature. Therefore, in the absence of target molecules, the report probe cannot assemble with the functionalized QD, leading to very low FRET signal. In the presence of the target molecules, binding of capture probe and report probe to the same target molecule places the complementary sequences in close proximity. Therefore, the

hybridization of the complementary sequences brings the acceptor close to the donor and generates FRET signal.

In the construction of the DNA nanosensor, QDs were utilized to serve as the nanoscaffold for capture probes and adjunct probes and as the donor in FRET. A number of capture probes and adjunct probes can be conjugated to a single QD. Therefore, a single QD carries multiple ligand molecules on its surface, resulting in stronger binding affinity to target molecules than individual ligands. In addition, the presence of multiple probes on the single QD improves the accessibility for assembly of the reporting probes. These functionalized QDs enable simultaneous assembly of several report probes on a single QD by capturing multiple target molecules. Thus, multiple FRET acceptors are placed on the surface of a single QD donor, leading to high FRET efficiency. Through modulating of the flexible linker length of the adjunct probe, I can manipulate the distance between acceptor and donor.

QDs present many advantages serving as the donor in this FRET system, including broad absorption spectra, high fluorescence quantum yield, and a narrow size distribution. I chose QD 605 and Cy5 as the donor and acceptor pair in the DNA nanosensor system because of the negligible crosstalk between the in emission spectra. The use of QD 605 allows for the selection of excitation wavelength far from the absorption spectra of Cy5, obviating the generation of background from direct excitation of Cy5.

2.3.2 Proof-of-principle for the nanosensor design

To demonstrate the principle of DNA nanosensor, we first chose a DNA sequence as a model DNA target molecule for optimization and detection.

The number of streptavidin molecules that are on the single QD and the concentration of QD solutions determine the maximum concentration of target that can be detected. In the proof-of-principle experiment, I typically used 2 nM (final concentration) functionalized QD solution. Assuming that each QD is conjugated with 15–25 streptavidins and there are 3 remaining biotin-binding sites on each streptavidin after its conjugation to QDs, in principle, up to 45–75 biotinylated probes (adjunct probe or capture probe) can be conjugated to a single QD 605. In this study, the ratio of adjunct probe to capture probe to QD 605 (15:15:1) is far from the saturable value of biotin-binding sites on a single QD. In Figure 2.3, the detection of a series of concentrations of model DNA target shows that the fluorescence intensity decreases at 605 nm and increases at 680 nm with the increase in concentration of the model DNA target. These results indicate the expected FRET.

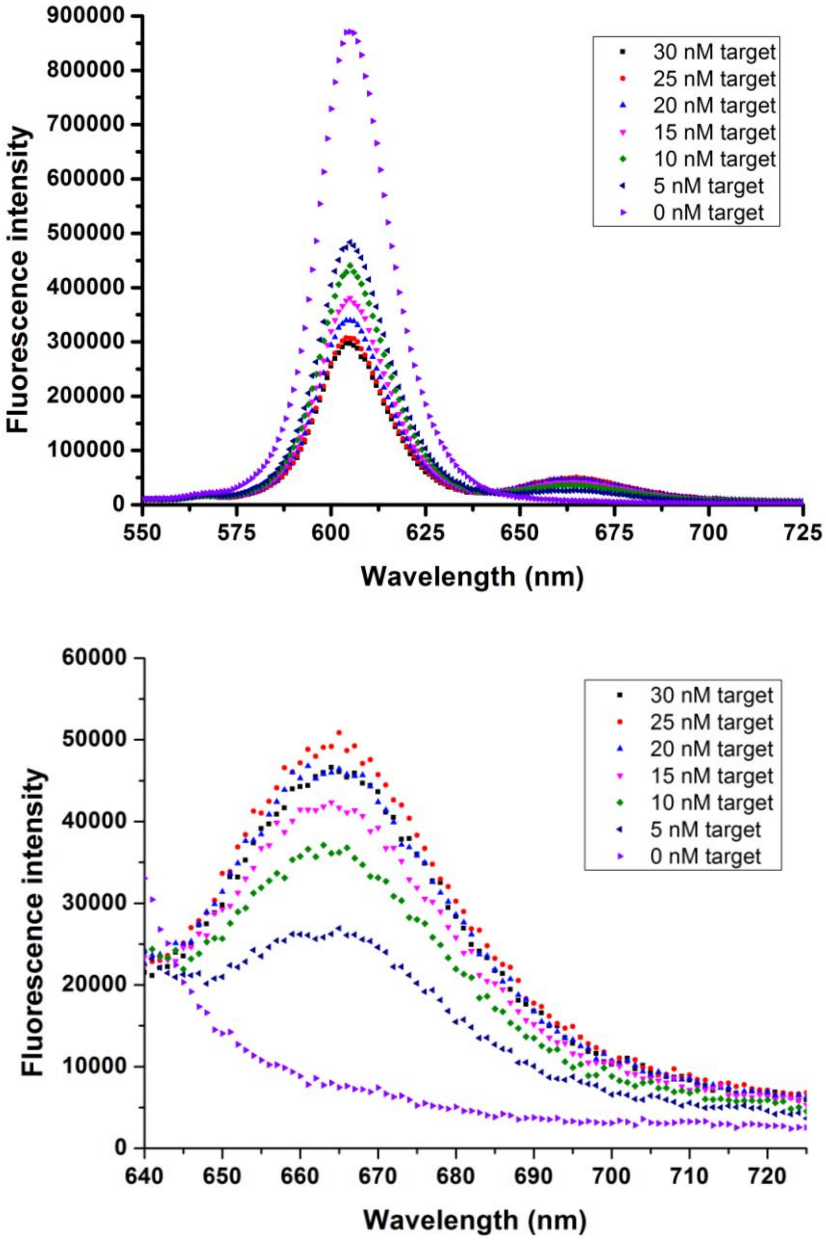

Figure 2.3 Bulk measurement of DNA binding-induced FRET.

Evolution of the fluorescence emission spectra from QD 605 and Cy5 as a function of the increasing concentration of the model DNA target (upper figure). The bottom figure shows the Cy5 fluorescence emission spectra. Excitation wavelength was at 475 nm.

Figure 2.4 shows that fluorescence emission at 680 nm due to FRET is at background levels for QD alone or QD and report probe. In the presence of the model DNA target, however, the emission at 680 nm is increased by several fold because of FRET.

According to the principle of sensor design, only by binding of the target to both the functionalized QD and the report probe can complementary sequences hybridize each other, which results in the QD donor and the Cy5 acceptor being brought into close proximity with each other, facilitating the FRET response. Figure 2.5 shows that a significant FRET signal is observed only when the functionalized QD, report probe, and target DNA are present to facilitate the binding-induced FRET. These results are consistent with the sensor design as illustrated in Figure 2.2.

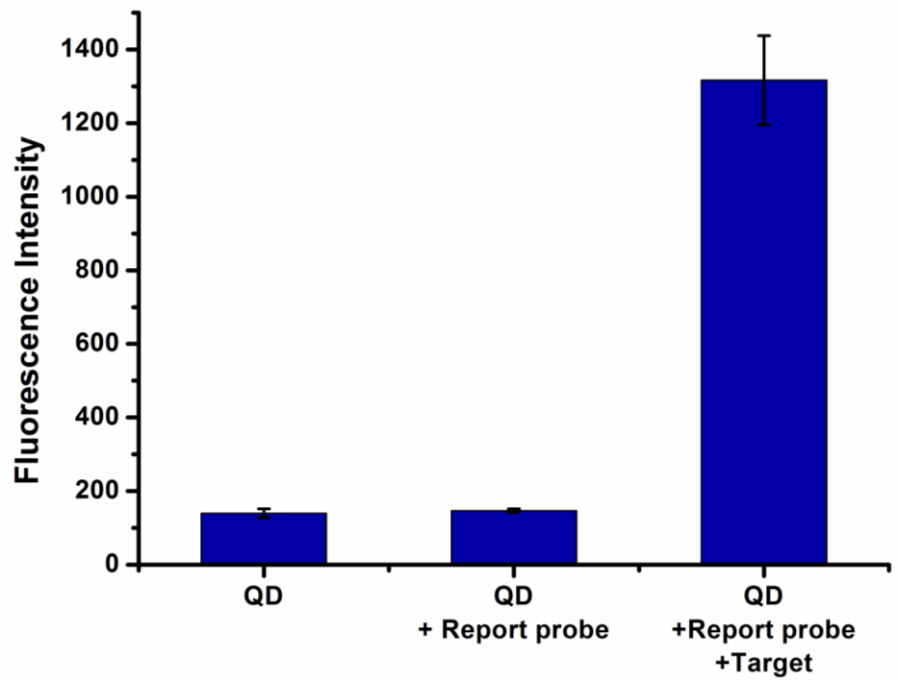

Figure 2.4 Comparison of background resulting from crosstalk and signal intensity

FRET signals for each sample in the presence of functionalized QD; both functionalized QD and report probe (control); and functionalized QD, report probe, and model DNA target (sample). Emission was monitored at 680 nm with excitation at 475 nm.

2.3.3 Optimization of DNA nanosensor for detection of the model DNA target

2.3.3.1 Background analysis

To optimize the performance of the DNA nanosensor, I examined the background source of the DNA nanosensor system. Figure 2.5 shows all possible sources of background. Among them, the adsorption of the adjunct probe on QD and report probe contributes significantly to the background. The overall objective of the optimization experiments was to achieve the maximum signal-to-background ratio. Determination of the model DNA target was used as a model system to optimize the various design and experimental parameters.

FRET efficiency and efficiency of hybridization are the two main factors which impact the signal-to-background ratio. The DNA nanosensor is mainly composed of three probes: adjunct probe, capture probe, and report probe. Two key factors of the adjunct probe should be taken into account. The first is the length and GC content of the complementary sequence on the adjunct probe which affects the efficiency of hybridization; the other one is the length of the flexible linker on the adjunct probe which influences the FRET efficiency.

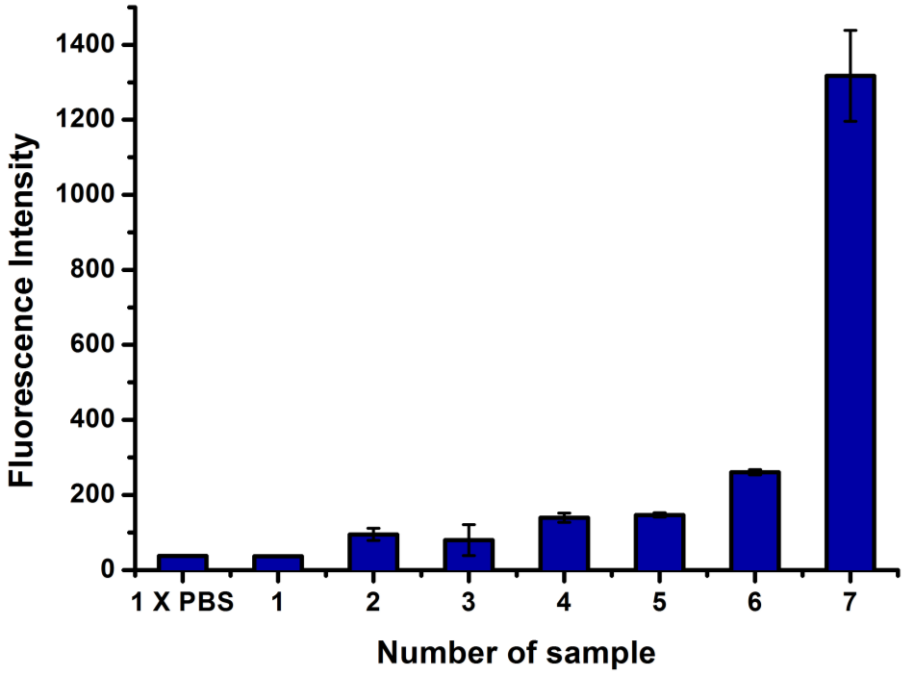

Figure 2.5 Analysis of various controls and a sample, showing the relative magnitude of overall background and signal

1: model DNA target only; 2: report probe only; 3: model DNA target and report probe; 4: functionalized QD only; 5: functionalized QD and model DNA target; 6: functionalized QD and report probe; 7: functionalized QD, report probe, and model DNA target.

2.3.3.2 Effect of the adjunct probe

In the process of optimization, I used fold change to express the FRET response, taking into account the signal-to-background ratio. The expression is shown in Section 2.2.2.

Optimization of the adjunct probe was focused on two factors: the length and GC content of the complementary sequence and the length of the flexible linker on the adjunct probe.

First, I optimized the length and GC content of the complementary sequence on the adjunct probe. The complementary sequences allow the adjunct probe would favor hybrid with the report probe within a limited local space, only in the presence of target which binds to both the report probe and the capture probe. Instead of direct hybridization of complementary sequences, the FRET signal is generated due to affinity ligands–target interaction as illustrated in Figure 2.2. Figure 2.6 shows the result from the use of the four types of oligonucleotides of adjunct probe (Table 2.1). Different FRET responses are obtained when the four adjunct probes with different length and GC content are used. The adjunct probe–C1 has the shortest length and the lowest GC content. Its hybrid with the complementary sequence has the lowest melting temperature (< 10 °C) in the absence of target binding. Therefore, the use of the C1 adjunct probe leads to the lowest background signal in the absence of the target DNA molecule. The low background results in the high signal-to-background ratio (fold change in FRET response).

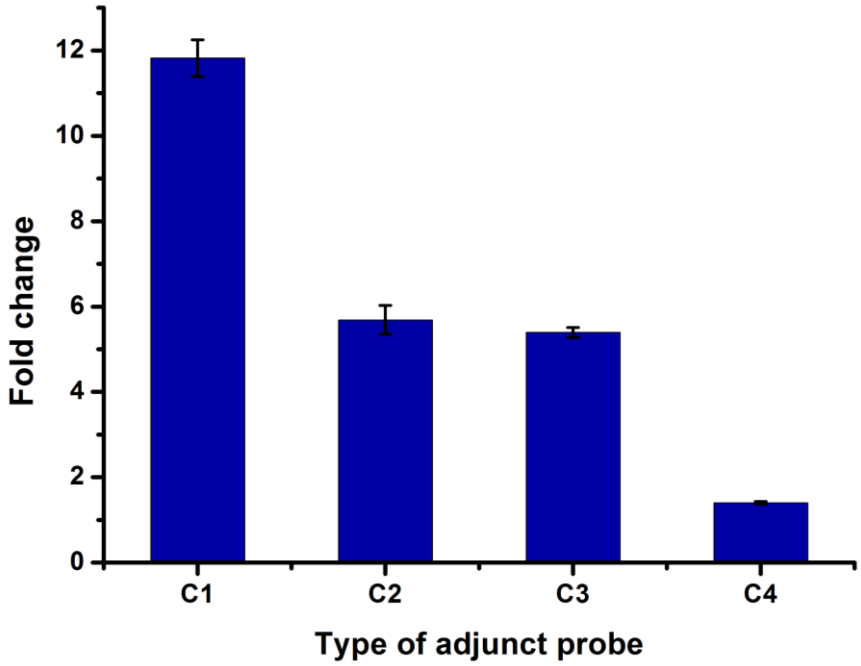

Figure 2.6 Comparison of four designs of the complementary sequences on the adjunct probe on the performance of the binding-induced DNA nanosensor.

C1: adjunct probe–C1; C2: adjunct probe–C2; C3: adjunct probe–C3; C4: adjunct probe–C4. Sequences of C1–C4 are shown in Table 2.1.

The concentration of adjunct probe was 10 nM. The concentration of capture probe was 10 nM. The concentration of report probe was 30 nM. The concentration of model DNA target was 30 nM.

Secondly, I tested the length of the flexible linker on the adjunct probe because this can affect FRET efficiency. Considering that FRET efficiency strongly depends on the donor–acceptor distance, the nanosensor design can control the donor–acceptor distance by adjusting the length of the flexible linker on the adjunct probe. Compared to the current nucleic acid–based fluorescence sensors that use the compact QD-biomolecule conjugate to reduce the FRET distance, this nanosensor design could achieve almost zero distance between donor and acceptor. Although the shorter length of flexible linker could improve the FRET efficiency, it also increases the steric effect which decreases the efficiency of hybridization between adjunct probe and report probe. However, the longer flexible linker is helpful for report probe to bind with adjunct probe, by offering more wide space. In our particular system (Figure 2.7), the Förster distance (R_0) is 6.94 nm. I tested the number of ploy T as flexible linker on adjunct probe from 2 to 18. Therefore, to study the effect of the flexible linker length, five types of adjunct probes with different length of poly T (2 nt, 6 nt, 10 nt, 14 nt, 18 nt) of flexible linker (Table 2.1) were compared, in order to find best FRET response (Figure 2.8).

To further explain why the length of flexible linker could influence the performance of the DNA nanosensor, we need to recognize that the transfer of energy from an excited-state donor fluorophore to a ground-state group. does not require direct contact. FRET efficiency (E) is the quantum yield of the energy transfer transition, which depends on the distance between the donor and the acceptor, the spectral overlap of the donor emission spectrum, the acceptor

absorption spectrum, and the relative orientation of both the donor and acceptor emission dipole moment. The Förster radius R_0 (a distance that produces 50% FRET efficiency) depends on both of the relative orientation and the spectral properties of the donor and acceptor fluorophores. When the donor and acceptor-labeled molecules undergo substantial and independent rotational motions, the orientation dependence is typically largely average (unless the transition dipoles for both species are highly constrained near-parallel to the membrane normal axis), and the value of R_0 depends principally on the fluorophore's spectral properties. R_0 values are of the order of 4–6 nm for donor-acceptor pairs commonly used for hetero-FRET experiments (in which the donor and acceptor fluorophores are different species).

Figure 2.8 shows the effect of length of flexible linker on the FRET efficiency using the flexible linker from 2T to 18T within 6nm. When using the 2T as the flexible linker, the FRET efficiency could reach the greatest FRET response. With the increase of length of flexible linker on adjunct probe, the FRET response decreases. These results are consistent with the above theoretical understanding of the system.

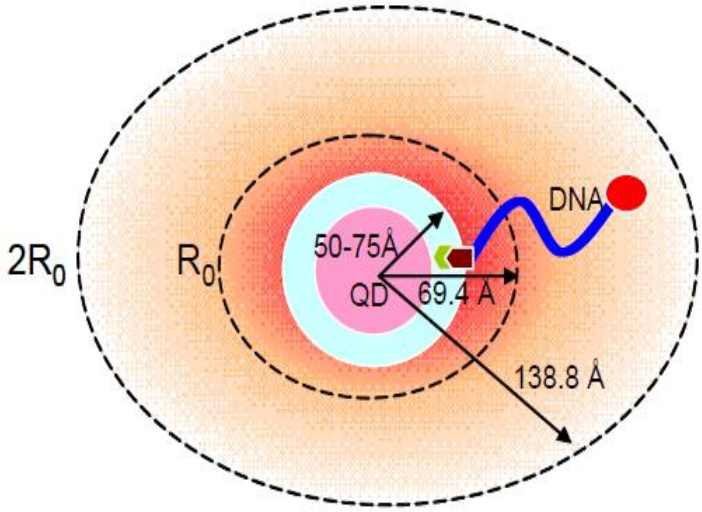

Figure 2.7 A schematic depicting the Förster distance (R_0) of an idealized streptavidin-functionalized 605QD donor and a Cy5 acceptor. The radius of this streptavidin-functionalized QD1 is 50-75 Å. The Förster distance R_0 is 69.4 Å. [8]

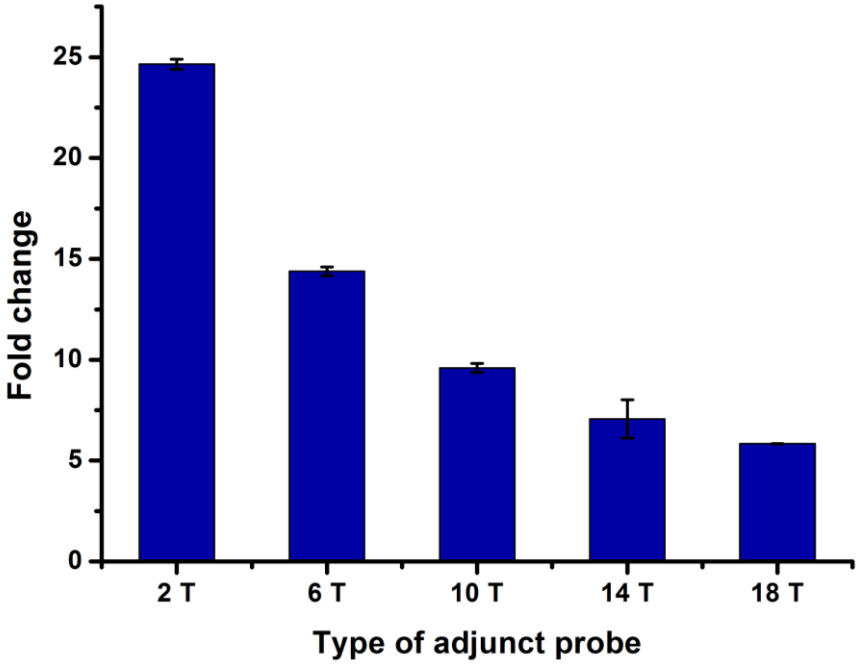

Figure 2.8 Effect of the length of flexible linker on the adjunct probe on the FRET response.

Comparison of five lengths of flexible linker on the adjunct probe on the performance of the binding-induced DNA nanosensor. 2T: Oligo of adjunct probe–2T; 6T: Oligo of adjunct probe–6T; 10T: Oligo of adjunct probe–10T; 14T: Oligo of adjunct probe–14T; 18T: Oligo of adjunct probe–18T;

The concentration of adjunct probe was 10 nM. The concentration of capture probe was 10 nM. The concentration of report probe was 30 nM. The concentration of model DNA target was 30 nM.

2.3.3.3 Effect of the capture probe

To test the influence of the number of capture probe conjugated on QD, I investigated both the ratio of adjunct probe to capture probe and the surface coverage on QD. To study the effect of the capture, I modified the QD surface with different concentrations of capture probes.

The results shown in Figure 2.9 demonstrate that the number of capture probes plays a crucial role. The FRET response increased as a result of the increase of concentration of capture probe until the ratio equals to 1 to 1. In this experiment, I changed the ratio of the capture probe to the adjunct probe, but kept the total number of probes on a single QD at 30. Beyond the summit (1:1), the FRET signal slowly decreased with the increase in the numbers of the capture probe.

The improvement of the FRET signal with the increase of the capture probe can be easily explained by the function of the capture probe to capture more of the target DNA onto the functionalized QD. The FRET response decreases when the ratio of capture probe to adjunct probe is beyond 1 to 1, which results the following two factors. First, the higher ratio of capture probe to adjunct probe weakens the density of adjunct probe on the QD due to the total number of probes on the QD, adjunct and capture, which remains constant (30/QD). Because the adjunct probe is responsible for capturing the report probe to generate the FRET signal, the decrease in the number of the adjunct probe leads to incomplete hybridization of the functionalized QD-target-report probe complexes with the adjunct probe when the adjunct probes have been saturated. Secondly, the higher

ratio of capture probe to adjunct probe increases the steric hindrance, preventing the hybridization of report probe and adjunct probe. The results show that when the ratio of capture probe to adjunct probe equals to 1:1, the FRET signal was optimized.

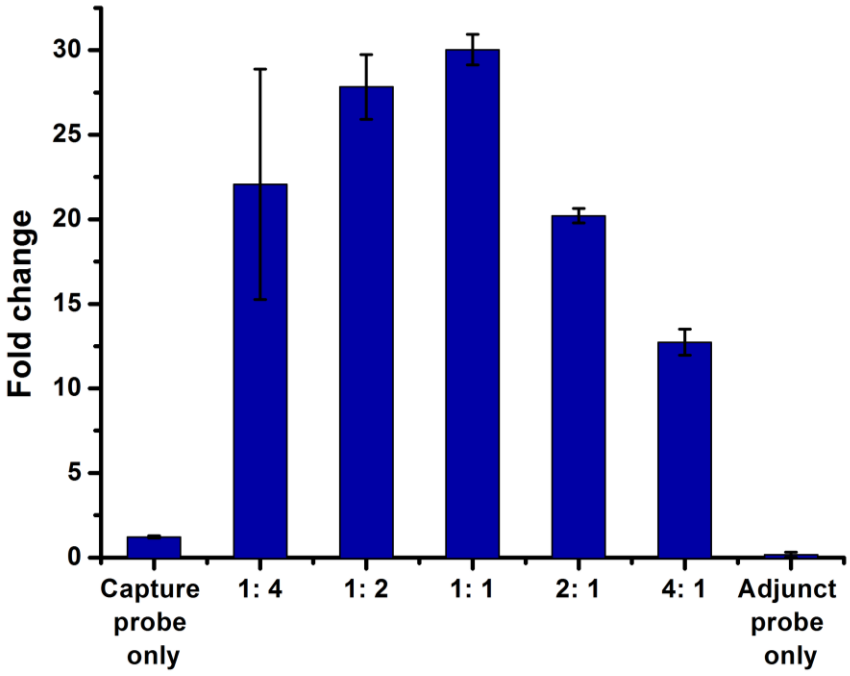

Figure 2.9 Effect of the ratio of capture probe to adjunct probe.

Comparison of seven ratios of capture probe to adjunct probe on 605 QD on the performance of the binding-induced DNA nanosensor. The concentration of model DNA target was 30 nM.

Another way to change the density of capture probe on the QD is the surface coverage of the adjunct probe on the QD. When I optimized the ratio of the capture probe to adjunct probe, I fixed the surface coverage of the QD at 30. To further explore the effect of capture probe density, I modified the quantum dot with different numbers of the capture probe from 1 to 30 on one quantum dot, keeping the ratio of capture probe to adjunct probe as 1:1. Notably, we could not control the exact number of probes on a single quantum dot. I adjusted the number of adjunct probes on the quantum dot by controlling the concentrations of the adjunct probe, the capture probe and quantum dot. With the increase in the number of the capture probe from 5 to 20, there was no significant enhancement in the FRET signal observed (Figure 2.10). For lower concentration of target, the QD could be modified with 5 capture probes and 5 adjunct probes. For higher concentrations of target, the QD could be modified with a larger number of both capture probes and adjunct probes (15~20), achieving similar FRET efficiency.

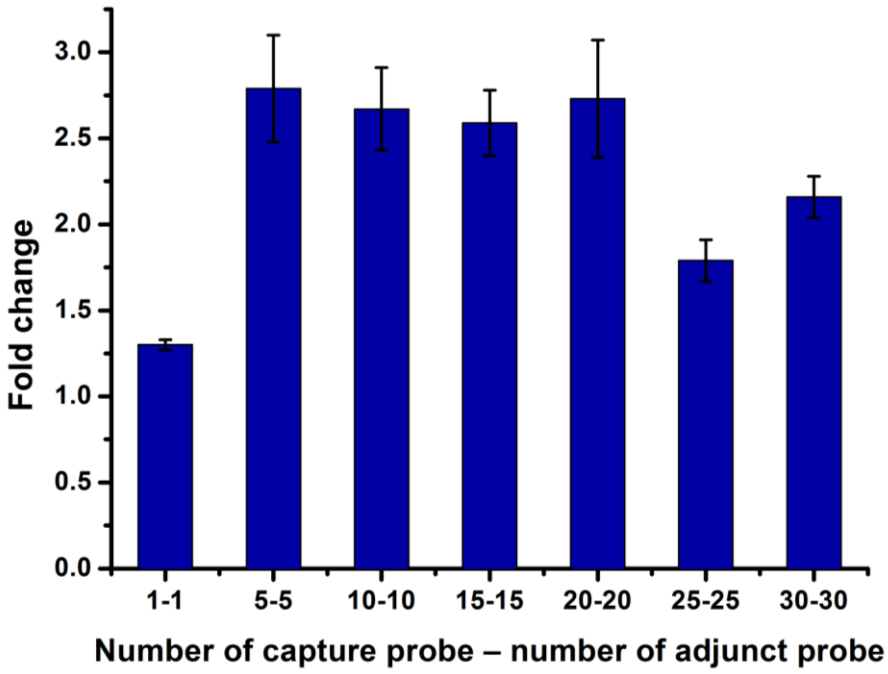

Figure 2.10 Effect of the number of capture probes on QD.

Comparison of different numbers of the capture probe on the QD 605 surface with the ratio of adjunct probe to capture probe fixed at 1:1. 1-1 represents the quantum dot conjugated with 1 adjunct probe and 1 capture probe theoretically. The concentration of model DNA target was 2 nM.

2.3.3.4 Effect of the ratio of quantum dot to report probe

A high concentration of the report probe could increase the sensitivity of detection with a constant dissociation constant (K_d). However, adsorption of the adjunct probe and report probe could result in high background FRET response.

Figure 2.11 shows the FRET response from 2 nM target DNA in a sample solution containing different concentrations of report probe. These results suggest that the optimum concentration of report probe is within the range from 2 nM to 10 nM. Within this range, for cost-effectiveness, we usually chose the concentration of report probe as 2 nM.

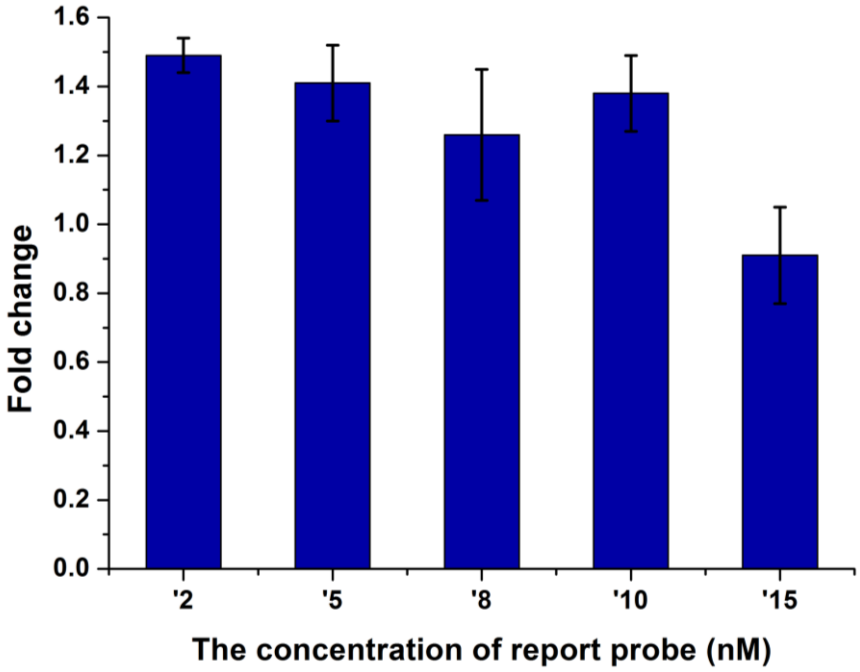

Figure 2.11 Effect of the concentration of the report probe on the FRET response.

Comparison of different ratios of functionalized QD to report probe on the performance of the binding-induced DNA nanosensor.

The concentration of adjunct probe was 5 nM. The concentration of capture probe was 5 nM. The concentration of model DNA target was 2 nM.

2.3.3.5 Effect of the final concentration of functionalized QD

Given that multiple report probes labeled with Cy5 could be attached to QD 605 by hybridization of complementary sequences on the capture probe and report probe, the QD 605 serves as the nanoscaffold to amplify the FRET signals. Serving as nanoscaffold, QD creates a high local concentration of complementary sequences, which thermodynamically favors the hybridization between adjunct probe and report probe. Fluorescence of Cy5 was detected of 680 nm due to the excitation of QD at 485 nm, which is far from the absorbance spectra of Cy5. However, QD 605 itself also had emission signal at 680 nm. In order to decrease the interference of QD 605 emission at 680nm, I optimized the concentration of functionalized QD. The results (Figure 2.12) demonstrate that 1 nm functionalized QD is the optimum condition.

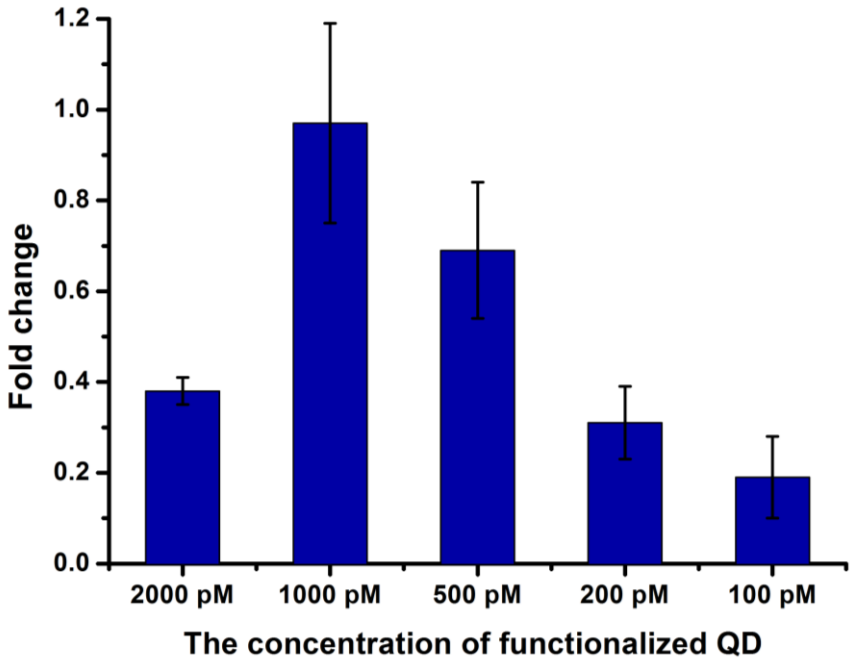

Figure 2.12 Effect of the concentration of functionalized QD on the FRET response. The concentration of model DNA target was 500 pM.

2.3.3.6 Determination of the model DNA target using the binding-induced DNA nanosensor

Figure 2.13 shows results from triplicate analyses of the model DNA target at eight concentrations (1–1000 pM). The sensitivity of the assay (FRET response change per unit of analyte concentration) was obtained from the slope of the calibration curve (Figure 2.13), where it is linear. Five repeats of the background (without model DNA target) sample were also measured. The limit of detection (LOD) was calculated as the analyte concentration corresponding to a FRET signal that was equal to blank + (standard deviation of the blank). The LOD was around 20 pM.

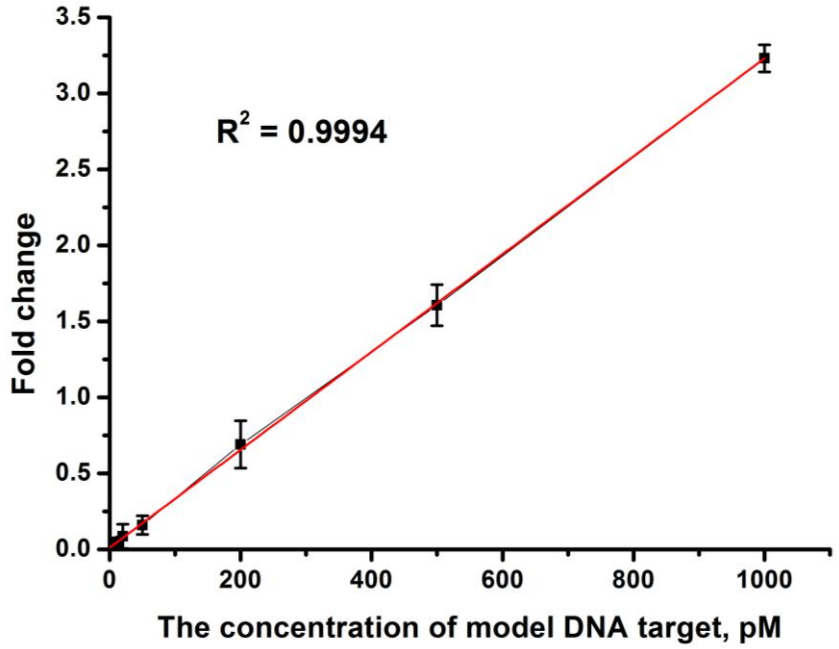

Figure 2.13 Detection of model DNA target.

FRET response from the detection of a model DNA target present at varying concentrations (0–1 nM). The error bars indicate the standard deviation. The incubation time was 30°C with 30 min.

The concentration of adjunct probe was 5 nM. The concentration of capture probe was 5 nM. The concentration of report probe was 30 nM. The concentration of model DNA target was 30 nM.

2.4 Conclusions

A new homogeneous assay strategy for detection of biomolecules has been developed using the binding-induced DNA assembly to generate fluorescence resonance energy transfer signal. A number of design parameters have been tested. Experimental conditions have been optimized. Under the optimum conditions, detection of a model DNA target could be achieved, with a detection limit of 20 pM. These experiments and sensor-design conditions form the basis for further development of similar sensors for DNA mutations (Chapter 3) and for proteins (Chapter 4).

2.5 References

1. Heyduk, E.; Dummit, B.; Chang, Y. H.; Heyduk, T. *Anal. Chem.* **2008,** *80,* 5152-5159.

2. Tyagi, S. and Kramer, F. R. *Nat. Biotechnol.* **1996,** *14,* 303-308.

3. Gill, R.; Zayats, M.; Willner, I. *Angew. Chem. Int. Edit.* **2008**, *47,* 7602-7625.

4. Castro, A. and Shera, E. B. *Anal. Chem.* **1995,** *67,* 3181-3186;

5. Weiss, S. *Science (Washington, DC)* **1999,** *283,* 1676-1683;

6. Shih, W. M.; Gryczynski, Z.; Lakowicz, J. R.; Spudich, J. A. *Cell (Cambridge, MA, U. S.)* **2000**, *102,* 683-694.

7. Qu, Q. and Sharom, F. J. *Biochemistry* **2001**, *40,* 1413-1422.

8. Zhang, C. Y.; Yeh, H. C.; Kuroki, M. T.; Wang, T. H. *Nat. Mater.* **2005,** *4,* 826-831.

Chapter 3: Detection of mutated p53 gene fragment using DNA nanosensor based on binding-induced fluorescence resonance energy transfer

3.1 Introduction

The objective of Chapter 3 is to demonstrate the capability of the DNA nanosensor based on binding-induced FRET for the detection of mutated a *p53* gene fragment, in particular, the detection of single-nucleotide polymorphism (SNP) in the *p53* gene sequence.

The *p53* acts as tumor suppressor gene. Many tumor point mutations within the gene have a dominant-negative effect [1]. The *p53* gene is not only a key part in the DNA damage response pathway, but also an important regulator in programmed cell death, differentiation, senescence, and angiogenesis [2-5]. The percentage of codon 248 on *p53* in single base substitutions is around 11% for mutations in cell-lines [6].

I have selected a 50-n.t. sequence of *p53*, encompassing the codon 248. I have obtained two 50-n.t. sequences, one containing a single nucleotide mutation in codon 248 (Figure 3.1 and Figure 3.2) and the other without mutation of this *p53* fragment. This chapter describes the development of an assay for the single nucleotide mutation in *p53*, using the assay strategy established in Chapter 2.

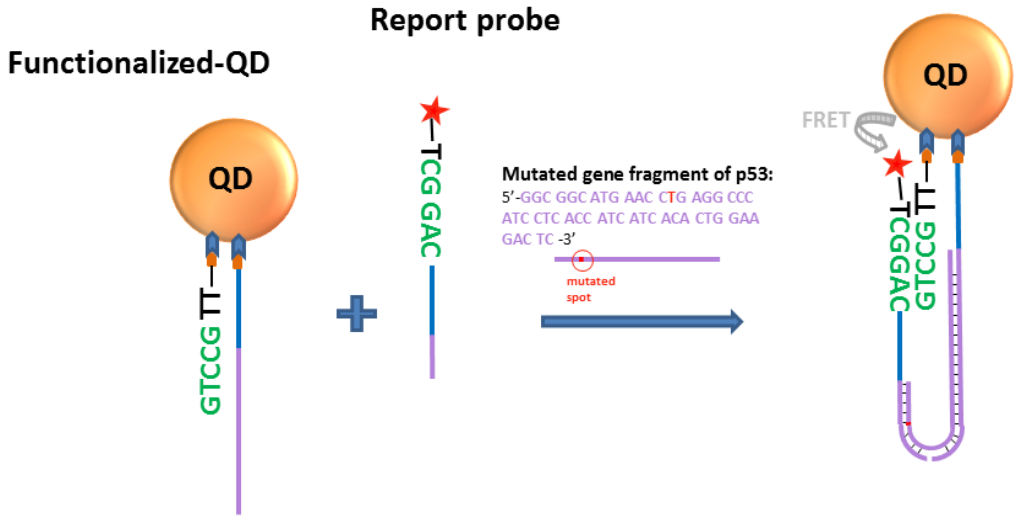

Figure 3.1 Schematic showing that hybridization of the mutated *p53* gene fragment to the complementary DNA on QD (Model 1) results in a stable DNA assembly which generates the FRET signal.

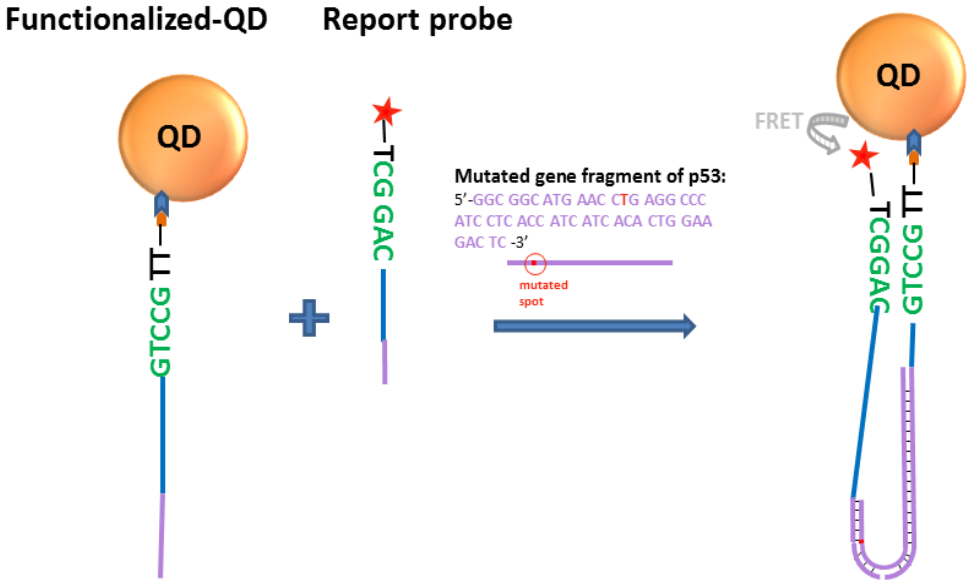

Figure 3.2 Schematic showing that hybridization of the mutated *p53* gene fragment to the complementary DNA on QD (Model 2) results in a stable DNA assembly which generates the FRET signal.

3.2 Experimental methods

3.2.1 Reagents

All solutions were prepared with phosphate buffered saline (1 × PBS) (137 mM NaCl, 10 mM phosphate, 2.7 mM KCl, pH 7.4) was diluted with deionized water from 10 × PBS buffer (Fisher Scientific, Nepean, ON). The oligonucleotides and DNA probes were obtained from Integrated DNA Technologies (Coralville, IA). Table 3.1 and Table 3.2 list the oligos used in this study. These oligos were all custom synthesized, labeled, and purified by IDT.

The oligos of the adjunct probe and capture probe were attached to a biotin group at the 5' end. The oligo of report probe was modified with Cy5 at the 3' end and biotin at the 5' end. The complementary sequences of the adjunct probe and report probe are highlighted in green in Table 3.1 and Table 3.2. The two complementary sequences of the mutated *p53* gene fragment are highlighted in purple. The streptavidin-functionalized QD 605 was supplied by Invitrogen (Carlsbad, CA). All other reagents were of analytical grade.

Table 3.1 DNA sequences used to construct the binding-induced DNA nanosensor (Model 1) for detection of the *p53* gene fragment and a single nucleotide mutation

DNA name	Sequences
Adjunct probe	**5'- Biotin-TT GCCTG -3'**
Capture probe	**5'- Biotin-TTT TTT TTT TTT TTT TTT TTT TTT TT GAG TCT TCC AGT GTG AT -3'**
Report probe 1	**5'- GCC TCA GGT TCA TTT TTT TTT TTT TTT TTT TTT TTT TTT TTT CAG GCT-Cy5-3'**
Report probe 2	**5'- GCC TCA GGT TC TTT TTT TTT TTT TTT TTT TTT TTT TTT TTT CAG GCT-Cy5-3'**
Wildtype *p53* gene fragment	**5'-GGC GGC ATG AAC CGG AGG CCC ATC CTC ACC ATC ATC ACA CTG GAA GAC TC-3'**
Mutated *p53* gene fragment	**5'-GGC GGC ATG AAC CTG AGG CCC ATC CTC ACC ATC ATC ACA CTG GAA GAC TC -3'**

The complementary sequences of the adjunct probe and report probe are highlighted in green. The complementary sequences which are affinity ligands of mutated *p53* gene fragment (target) are highlighted in purple. The mutated point is highlighted in red. The flexible linkers of the adjunct probe are highlighted in blue.

Table 3.2 DNA sequences used to construct the binding-induced DNA nanosensor (Model 2) for detection of the *p53* gene fragment and a single nucleotide mutation

DNA name	Sequences
Combined adjunct probe and capture probe	**5'- Biotin-TTG CCT GTT TTT TTT TTT TTT TTT TTT TTT GAG TCT TCC AGT GTG AT -3'**
Report probe 2	**5'- GCC TCA GGT TC TTT TTT TTT TTT TTT TTT TTT TTT TTT TTT CAG GCT-Cy5-3'**
Mutated *p53* gene fragment	**5'-GGC GGC ATG AAC CTG AGG CCC ATC CTC ACC ATC ATC ACA CTG GAA GAC TC -3'**

The complementary sequences of the adjunct probe and report probe are highlighted in green. The complementary sequences which are affinity ligands of mutated *p53* gene fragment (target) are highlighted in purple. The mutated point is highlighted in red. The flexible linkers of the adjunct probe are highlighted in blue.

3.2.2 Stock solutions

All stock oligo solutions were diluted with 1 × PBS in 1000 μL micro-centrifuge tubes to a concentration of 50 nM. They were stored at -20 °C when not in use.

3.2.3 Preparation of a DNA nanosensor based on binding-induced FRET for the optimization and detection of mutated a *p53* gene fragment

To prepare a nanosensor for analysis of the mutated *p53* gene fragment, I designed the partially complementary sequences as affinity ligands of the mutated *p53* gene fragment target. I prepared functionalized QD (in Model 1 nanosensor) with 150 nM biotinylated capture probe, 150 nM biotinylated adjunct probe, and 10 nM QDs in 1 × PBS buffer. Similarly, I prepared functionalized QD (in Model 2 nanosensor) with 15 nM biotinylated combined adjunct probe and capture probe and 10 nM QDs in 1 × PBS buffer. Then, functionalized QD solutions were incubated at 37 °C for 30 min and then at room temperature for another 10 min.

To illustrate the sensitivity and to generate a calibration for the detection of the mutated *p53* gene fragment, I incubated various concentrations of the mutated *p53* gene fragment with 1 nM functionalized QD and 2 nM report probe in 1×PBS buffer. The sample solutions were incubated at 37 °C for 30 min. The fluorescence signals from each of these sample solutions (three parallel samples) were read out by using a DTX 880 multimode detector.

To test the specificity of the assay, I compared the analyses of the mutated *p53* gene fragment (5 nM) and wild type *p53* gene fragment (5 nM). Each of these

was incubated with a mixture of 1 nM functionalized QD and 5 nM report probe in 1 × PBS buffer. The corresponding blank solutions contained all the reagents but not the *p53* gene fragment. The final sample and blank solutions were incubated at 37 °C 30 min before analysis on a DTX 880 multimode detector. The final volume of the sample solutions was 100 μL. The fold change of fluorescence response was evaluated.

3.3 Results and Discussion

3.3.1 DNA nanosensor based on binding-induced FRET for detection of a mutated *p53* gene fragment

Using the strategy described in Chapter 2, I have designed two assays (Figure 3.1 and Figure 3.2) to detect *p53* containing a single nucleotide mutation in codon 248 of the *p53* gene. The first design (Figure 3.1) is similar to that as described in Chapter 2 (Figure 2.1), and it contains the functionalized QD with the adjunct probe and capture probe. In the second design (Figure 3.2), the adjunct probe and capture probe are combined in a single piece of oligonucleotide (see Table 3.2 for sequence).

3.3.2 Optimization of DNA nanosensor

Given that all of the optimized conditions of the DNA nanosensor in Chapter 2 are based on the detection of the model DNA sequence, most of the optimum conditions can be applied to the design of DNA nanosensor for detection of the mutated *p53* gene fragment. However, the design of report probe and

incubation temperature should be further optimized because the report probe is designed based on a specific target. Besides, the length of report probe influences the performance of DNA nanosensor at different incubation temperatures.

Figure 3.3 shows the FRET response from the analyses of the mutated *p53* gene fragment (5 nM) and wildtype *p53* gene fragment (5 nM), comparing the incubation temperature at 25 °C and 37 °C. The bigger difference in the FRET response between the mutated *p53* gene fragment and wildtype *p53* gene fragment was generated at 37 ℃ compared to 25 °C. Therefore 37 °C was chosen as the incubation temperature.

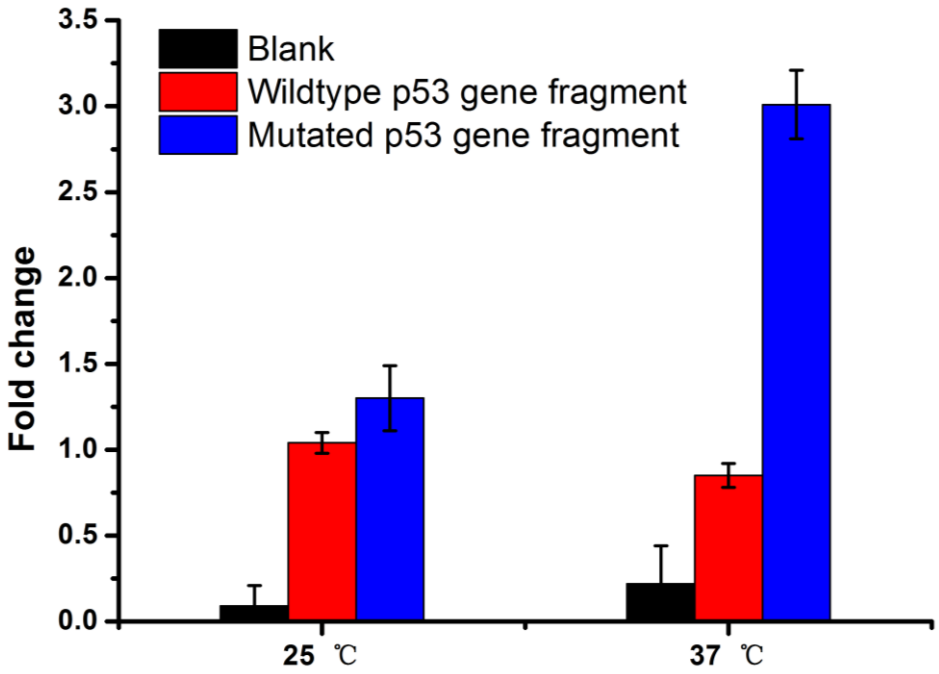

Figure 3.3 Effect of incubation temperature on the detection of the mutated *p53* gene fragment.

The sample solutions contained 5 nM of either the mutated *p53* gene fragment or the wildtype *p53* gene fragment, 1 nM functionalized the QD, and 10 nM report probe 1. The blank solutions contained all the reagents but not *p53* gene fragment. The incubation time was 30 min.

Incubated at the optimum temperature (37 °C), the sample solution was detected with two types of report probes (report probe 1 and report probe 2 in Table 3.1). The results (Figure 3.4) demonstrate that report probe 2 has achieved the better discrimination between wildtype and mutated *p53* gene fragments. So the report probe 2 was chosen for the SNP detection of the mutated *p53* gene fragment.

In order to simplify the DNA nanosensor structure, I combined the adjunct probe and capture probe, forming the DNA nanosensor design (Model 2 as shown in Figure 3.2). Compared to the original design (Figure 3.1), Model 2 decreases the surface coverage on QD, which increases the efficiency of hybridization of complementary sequences on the adjunct probe and report probe. However, Model 2 fixed the ratio of adjunct probe to capture probe as 1:1, which could reduce an option of decreasing background, particularly for ultrasensitive detection. However, for the detection of target at relatively high concentration (5 nM), Figure 3.5 shows similar performance between the two designs of the DNA nanosensor.

Therefore, the optimized conditions of the DNA nanosensor for detection of the mutated *p53* gene fragment were as follows: incubation of the sample solution at 37 °C for 30 min, and the ratio of adjunct probe to capture probe to report probe was 1:1:2.

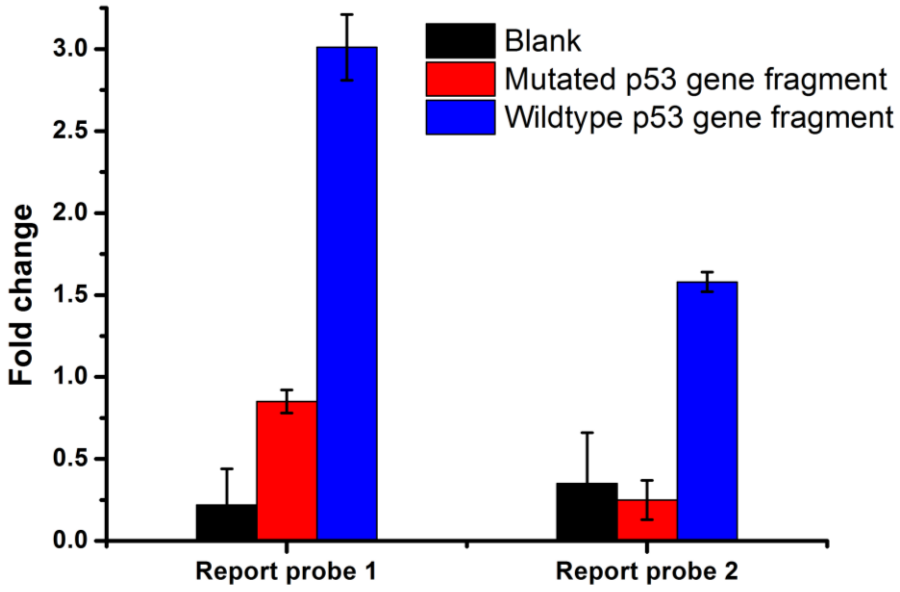

Figure 3.4 Effect of the type of report probe on the detection of the mutated *p53* gene fragment.

The sample solutions contained 5 nM of either the mutated *p53* gene fragment or the wildtype *p53* gene fragment, 1 nM functionalized QD, and 10 nM report probe 1 (or report probe 2). The blank solutions contained all the reagents but not the *p53* gene fragment at 37 °C. The incubation time was 30 min.

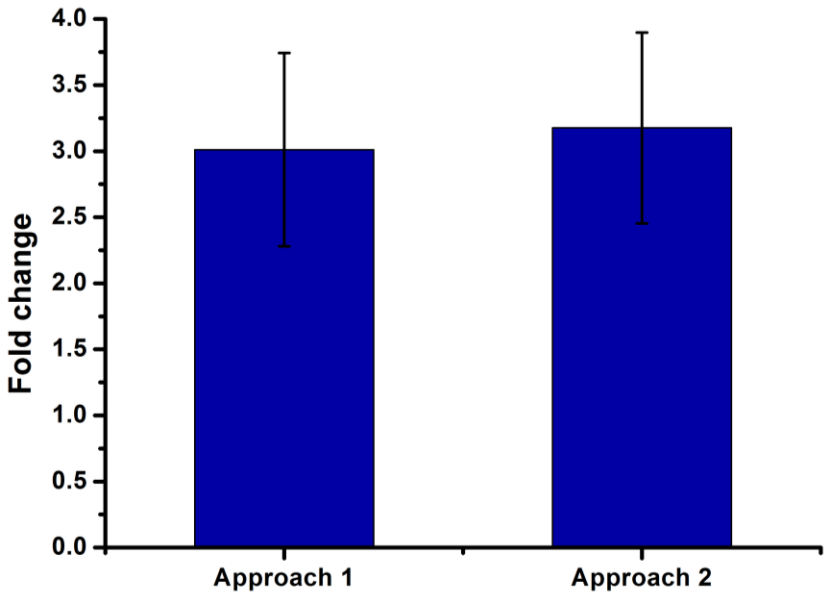

Figure 3.5 Comparison of two types of DNA nanosensor design for the detection of the mutated *p53* gene fragment.

The incubation conditions were the same as shown in Figure 3.4

3.3.3 Sensitive and specific detection of the mutated *p53* gene fragment using DNA nanosensor

Under the optimum conditions, the performance of the DNA nanosensor for sensitive detection of the mutated *p53* gene fragment is shown in Figure 3.6. The detection limit was 50 pM.

The specificity of the DNA nanosensor for the mutated *p53* gene fragment is assured by the requirement of three molecular events (the recognition of the mutated *p53* gene fragment by each of the two probes separately and the association of the complementary sequences). In the absence of any one of these, the sensor will not generate a signal. Only perfectly complementary targets elicit this FRET response, as hybridization does not occur when the target contains a mismatched nucleotide or a deletion. As shown in Figure 3.7, a small FRET signal was observed in the absence of target (control); this small FRET signal might result from the target-independent association between the adjunct probe and report probe. In the presence of the wildtype *p53* gene fragment, no significant difference in the FRET signal was observed compared to the control group, suggesting no binding-induced FRET response was generated. However, in the presence of 1-base mismatched mutated *p53* gene fragment, the normalized FRET response increased dramatically than when in the presence of the wildtype *p53* gene fragment, suggesting the high selectivity of the DNA nanosensor based on binding-induced FRET.

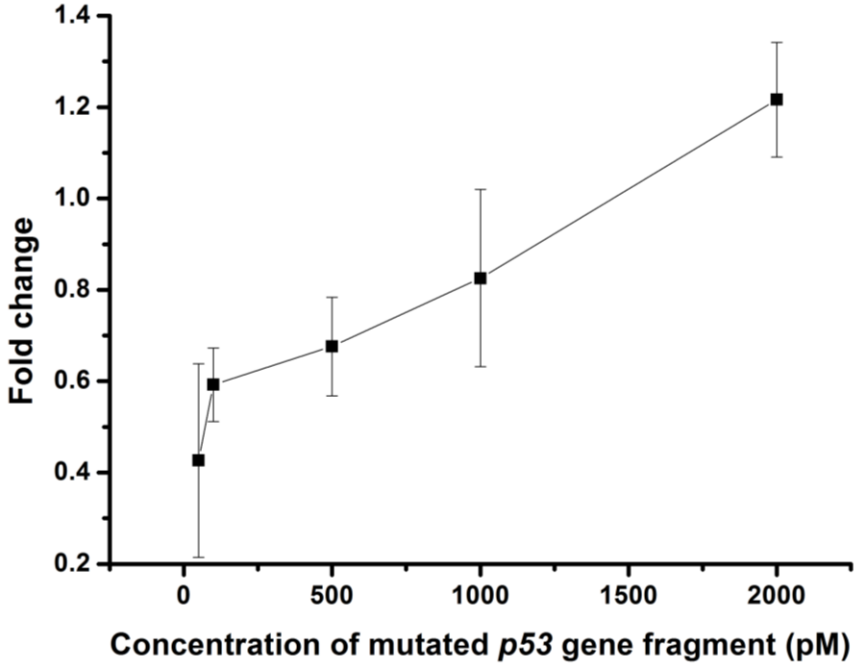

Figure 3.6 Determination of the mutated p53 gene using the binding-induced FRET assay. The concentration of adjunct probe was 5 nM. The concentration of capture probe was 5 nM. The concentration of report probe was 2 nM.

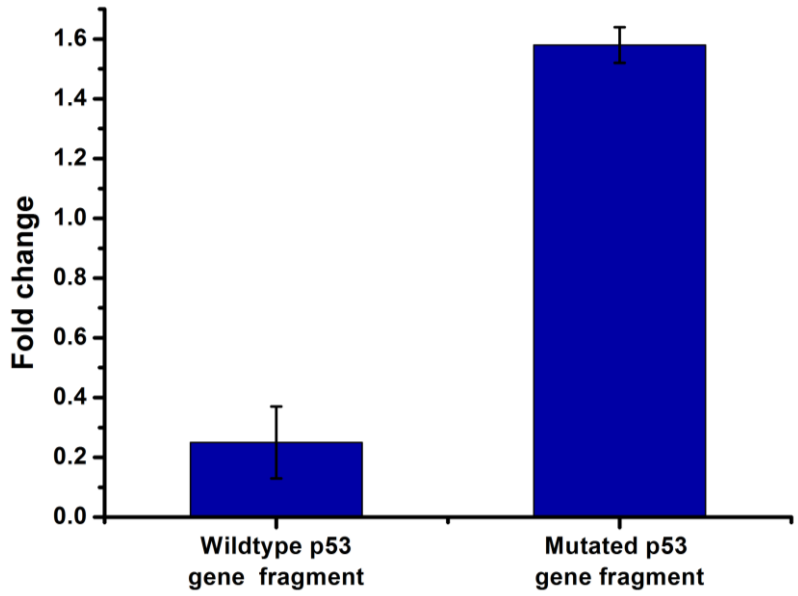

Figure 3.7 Detection of a single-nucleotide polymorphism (SNP) in the *p53* gene fragment.

3.4 Conclusions

The sensitive and specific detection of the mutated *p53* gene fragment has been achieved by using the DNA nanosensor based on binding-induced FRET. This approach could be used for detecting other single-nucleotide polymorphisms SNPs in other genes. Additionally, according to the different targets, the length of report probe could be adjusted, which allows for the use of different incubation temperatures to facilitate specific assays. Two types of DNA nanosensor design could achieve similar detection of the mutated *p53*.

3.5 References

1. Milner, J.; Medcalf, E. A.; Cook, A. C. *Mol. Cell. Biol.* **1991**, *11,* 12-19.

2. Rotter, V.; Alonigrinstein, R.; Schwartz, D.; Elkind, N. B.; Simons, A.; Wolkowicz, R.; Lavigne, M.; Beserman, P.; Kapon, A.; Goldfinger, N. *Seminars in Cancer Biology* **1994**, *5*, 229-236.

3. Wynford-Thomas, D. *J. Pathol.* **1999,** *187,* 100-111.

4. Vojta, P. J. and Barrett, J. C. *Biochim. Biophys. Acta.* **1995**, *1242,* 29-41.

5. Bouck, N. *Biochim. Biophys. Acta.* **1996,** *1287,* 63-66.

6. Petitjean, A.; Mathe, E.; Kato, S.; Ishioka, C.; Tavtigian, S. V.; Hainaut, P.; Olivier, M. *Hum. Mutat.* **2007,** *28,* 622-629.

Chapter 4: Detection of PDGF using the DNA nanosensor based on binding-induced fluorescence resonance energy transfer

4.1 Introduction

Given that proteins play an important role in life science, specific and sensitive protein detection in homogeneous solution attracts increasing attention [1, 2]. The study of oncoproteins which are often found overexpressed or mutated in cancer growth tissue can lead to new biomarkers used for early cancer diagnosis [3]. Platelet-derived growth factor (PDGF) was discovered as a major mitogen and act as an oncoprotein [4-6]. PDGF is composed of two polypeptide chains, which are linked by a disulfide bond [7]. PDGFs are classified as the homodimers PDGF-AA or PDGF-BB or the heterodimer AB, which are differentially expressed in different kinds of cells and their biological functions are mediated through binding to PDGF receptors α and β that function as cell surface proteins [8-10]. Because the interaction between PDGF and the PDGF receptors is essential to understand their functions in malignant tumors, the specific detection of PDGF-BB is necessary for providing insight into the molecular basis of cancer. The receptor β binds to the PDGF-AB and PDGF-BB with high affinity, whereas the receptor α binds to all three isomers [11-13]. Although most traditional bioanalytical methods use antibodies for recognition of

these proteins, recent approaches based on the use of aptamers have also been demonstrated for the determination of PDGF [14-18].

The objective of Chapter 4 is to demonstrate an application of the binding-induced FRET sensor for the detection of protein and for the discrimination of protein isomers. I chose the PDGF-BB as a model protein target because aptamers for this protein are available. In addition, taking advantage of the property that some aptamers bind only to the B chain of PDGF [19], we should be able to discriminate between PDGF isomers by conjugating proper aptamers on the DNA nanosensor.

4.2 Experimental methods

4.2.1 Reagents

Phosphate buffered saline (1 × PBS) (137 mM NaCl, 10 mM phosphate, 2.7 mM KCl, pH 7.4) was diluted with deionized water from 10 × PBS buffer (Fisher Scientific, Nepean, ON). The oligonucleotides and DNA probes were obtained from Integrated DNA Technologies (Coralville, IA). Table 4.1 lists the oligos used in this study. These oligos were all custom synthesized, labeled, and purified by IDT.

The oligo of the adjunct probe and capture probe had to a biotin group attached to the 3’ end. The oligo of report probe was modified with Cy5 at the 5’ end and biotin at the 3’ end. The complementary sequences of the adjunct probe and report probe are highlighted in green in Table 4.1. The aptamer sequences are

highlighted in purple. The streptavidin-functionalized 605 QD was supplied by Invitrogen (Carlsbad, CA). All other reagents were of analytical grade.

Table 4.1 DNA sequences used to construct the binding-induced DNA nanosensor for detection of platelet-derived growth factor (PDGF)

DNA name	**Sequences**
Adjunct probe	5'- **GTCCGTT**-Biotin -3'
Capture probe	5'-Biotin-**TTT TTT TTC ACA GGC TAC GGC ACG TAG AGC ATC ACC ATG ATC CTG TG**-3'
Report probe	5'-**Cy5**-**TCG GAC ATT ATT TTT TTT TTT TTT TTT TTT TAC TCA GGG CAC TGC AAG CAA TTG TGG TCC CAA TGG GCT GAG TA**-3'

Complementary bases are highlighted in green on the adjunct probe and report probe. The sequences highlighted in purple are aptamers for PDGF-BB. The flexible linkers on adjunct probes are highlighted in blue.

Table 4.2 K_d values for two aptamers binding to PDGF variants

affinity ligand	PDGF-AA	PDGF-BB
aptamer (36t)	72 ± 12	0.093 ± 0.009
aptamer (41t)	49 ± 8	0.129 ± 0.011

Data from Green L.S.; Jellinek, D.; Jenison, R.; Ostman, A.; Heldin, C. H.; Janjic, N. *Biochemistry* **1996,** *53,* 14413 – 14424

4.2.2 Stock solutions

All stock oligo solutions were diluted with 1 × PBS in 1000 μL micro-centrifuge tubes to a concentration of 50 nM. They were stored at -20 °C when not in use.

4.2.3 Preparation of a DNA nanosensor based on binding-induced FRET for the detection of PDGF-BB

To prepare a nanosensor for analysis of PDGF-BB, I prepared functionalized QD with 50 nM biotinylated capture probe, 200 nM adjunct probe, and 10 nM QDs in 1 × PBS buffer solution with the addition of $MgCl_2$ (1 mM) Then, functionalized QD were incubated at 37 °C for 30 min and then at room temperature for another 10 min.

To study the effect of the incubation temperature on the detection of PDGF-BB, I measured the FRET response of PDGF-BB (10 nM) after its incubation with the same concentrations of report probes and functionalized QD in the incubation buffer (1 × PBS, 1 mM $MgCl_2$). The temperature was either 25 °C or 37°C. The mixed solution was maintained at each temperature for 30 min before the FRET response was measured. The total sample volume was 100 μL.

To study the effect of the ratio of capture probe to report probe on the detection of PDGF-BB, I prepared parallel samples (10 nM PDGF-BB) and blank solutions as follows. Keeping the ratio of capture probe to adjunct probe to QD at 15:15:1 on the functionalized QD, I incubated the sample and blank solutions with varying ratios of capture probe to report probe (3:2, 3:10, 3:20, 3:40) in the

incubation buffer (1 × PBS, 1mM $MgCl_2$). The solutions were incubated at 25 °C for 30 min before FRET measurement.

To study the effect of the numbers of adjunct probe and capture probe on QD, I used the optimized ratio of capture probe to report probe (3:2) for the analysis of the sample (5 nM PDGF-BB) and blank solutions. Then the number of capture probe and report probe on QD was changed from capture probe only to 30 capture probes and 5 adjunct probes on average. The sample and blank solutions were incubated at 25 °C for 30 min before FRET measurement.

To illustrate the sensitivity and to generate a calibration for the detection of PDGF-BB, I incubated various concentrations of PDGF-BB with 1 nM functionalized QD and 5 nM aptamer report probe in 1 × PBS buffer with the addition of $MgCl_2$ (1 mM). The sample solutions were incubated at room temperature for 30 min. The fluorescence signals from each of these sample solutions (three parallel samples) were read out by using a DTX 880 multimode detector.

To test the specificity of the assay, I compared the analyses of PDGF-AA (5 nM), PDGF-AB (5 nM), and PDGF-BB (5 nM). Each of these was incubated with a mixture of 1 nM functionalized QD and 5 nM report probe in 1 × PBS buffer solution with the addition of $MgCl_2$ (1 mM). The final volume of the sample solution was 100 μL. The corresponding blank solutions (100 μL) contained all the reagents but not PDGF. The sample and blank solutions were incubated at room temperature for 30 min before analysis on a DTX 880 multimode detector. The fold change of fluorescence response was evaluated.

4.3 Results and Discussion

4.3.1 The DNA nanosensor based on binding-induced FRET for detection of PDGF-BB

Figure 4.1 shows schematically a binding-induced FRET assay for PDGF-BB. Specific aptamers (41t and 36t) recognizing PDGF-BB were used for the binding [80-82]. The capture probe consisted of an aptamer (36t) that was conjugated to the QD 605. An adjunct probe, with the same sequence described previously in Chapters 2 and 3, was also conjugated to the QD. The report probe was a second aptamer (41t) that was linked at the 5'-end to Cy5.

Each B chain of the PDGF binds to an aptamer. Binding of PDGF-BB to the aptamer on the QD and to the aptamer on the report probe promotes the hybridization of the complementary sequences. This binding-induced hybridization brings the fluorescent Cy5 to close proximity with QD, facilitating FRET from the QD to Cy5. The detectable FRET response is a measure of the PDGF-BB in the solution.

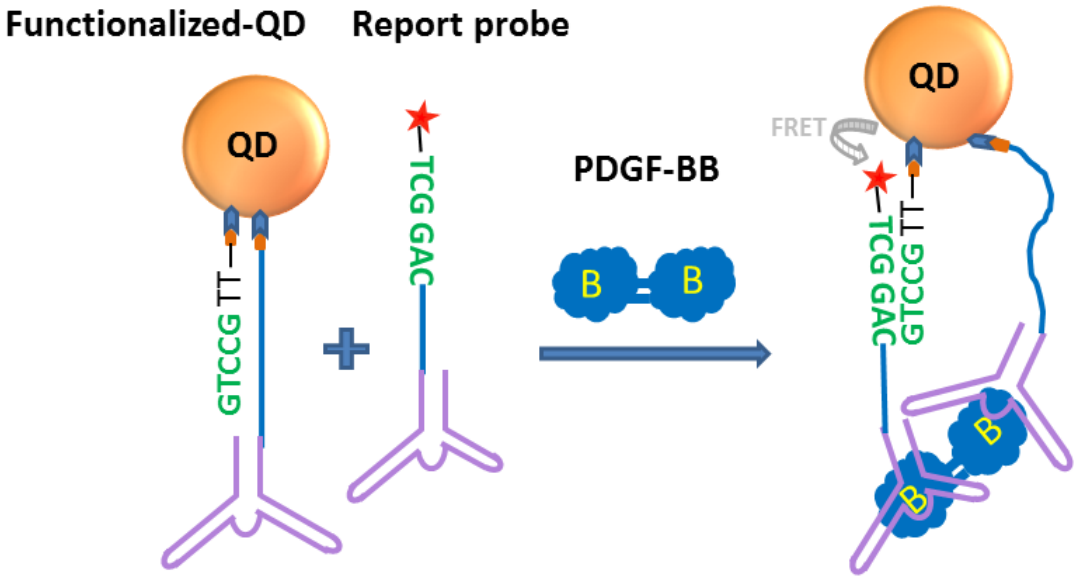

Figure 4.1 Schematic showing that binding of PDGF-BB to DNA aptamers results in a stable binding-induced DNA assembly which generates the FRET signal.

Aptamer functionalized capture probe and adjunct probe are each conjugated to the QD 605. The report probe is labeled with Cy5 and at the 5'-end. The binding of PDGF-BB to two DNA aptamers assembles the report probe onto the QD 605 scaffold, resulting in FRET between QD 605 and Cy5.

4.3.2 Optimization of the DNA nanosensor

The temperature of incubation plays a critical role in the binding between aptamers and PDGF-BB and in the hybridization of complementary sequences. The effect of incubation temperature on the detection of PDGF-BB was studied. The results comparing incubation at 37 °C and 25 °C are shown in Figure 4.2. A higher FRET response was obtained at an incubation temperature of 25 °C. The FRET response obtained at 37 °C was almost half compared to that obtained at 25 °C. Therefore, the incubation temperature of 25 °C was chosen for the detection of PDGF-BB.

Figure 4.3 shows the FRET response from the analyses of 10 nM PDGF-BB in the solutions containing various ratios of capture probe to report probe. The FRET response decreased with the decrease of ratio of capture probe to report probe. The highest FRET response was obtained when the ratio was 3:2. Therefore, 3:2 was chosen as the ratio of capture probe to report probe.

Figure 4.4 presents the FRET response from the analysis of 5 nM PDGF-BB when a varying number of capture probe and adjunct probes were used. The highest FRET response was produced with 20 capture probes and 5 adjunct probes on QD. So this condition was chosen for the sensitive detection of PDGF-BB.

In summary, the optimized ratio of the adjunct probe, capture probe, report probe and QD was 5:20:13:1. The optimum incubation conditions were 25℃ for 30 min in the 1 × PBS buffer with 1 mM $MgCl_2$.

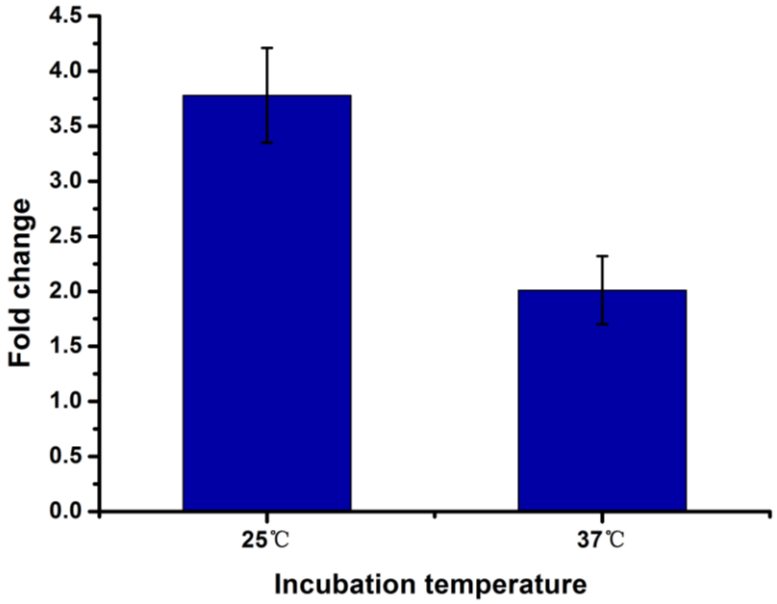

Figure 4.2 Effect of incubation temperature on the detection of PDGF-BB.

The sample solutions contained 10 nM PDGF-BB, 15 nM biotinylated capture probe, 15 nM biotinylated adjunct probe, 1 nM QD, and 50 nM report probes. The buffer solution was 1 × PBS with the addition of 1 mM $MgCl_2$. The incubation time was 30 min.

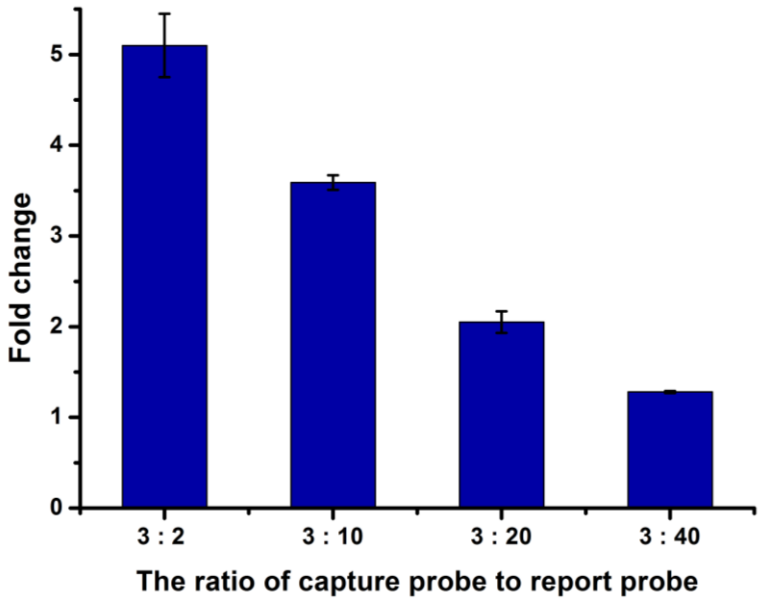

Figure 4.3 Effect of the ratio of capture probe to report probe on the FRET response from the analysis of PDGF-BB.

The sample solutions contained 10 nM PDGF-BB. The functionalized QD were prepared with the ratio of capture probe to adjunct probe at 1:1. The sample solutions were incubated at 25 °C for 30 min before FRET measurement.

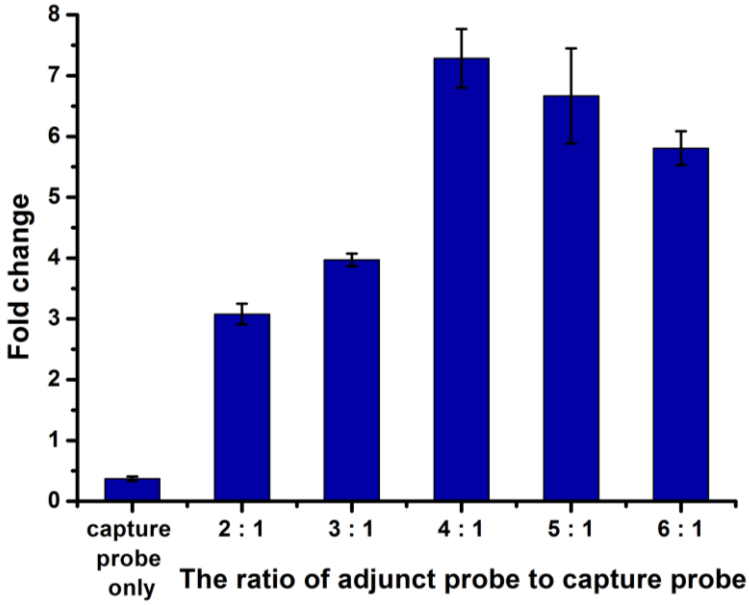

Figure 4.4 Effect of the ratio of adjunct probe to capture probe on the FRET response from the analysis of PDGF-BB.

The sample solutions contained 5 nM PDGF-BB. The ratio of capture probe to report probe was kept at 3:2.

4.3.3 Determination of the PDGF-BB using the binding-induced FRET assay

Figure 4.5 shows the FRET response from the analysis of PDGF-BB at a series of concentrations (156 pM - 5 nM). These results indicate that the FRET signals are responsive to PDGF-BB concentrations. This assay format based on binding-induced FRET allows detection of the PDGF-BB protein with around 600 pM limit of detection.

4.3.4 Discrimination between PDGF variants using the binding-induced FRET assay

PDGF consists of an A chain and/or a B chain. The two aptamers (41t and 36t) preferentially bind to the B chain of PDGF. Therefore, PDGF-BB can bind to both aptamers; PDGF-AB can bind to a single aptamer; and PDGF-AA has much weaker binding to the aptamers. Based on these binding differences, we are able to differentiate the PDGF variants.

Figure 4.6 compares the FRET responses from the parallel analyses of reagent blank (without PDGF), PDGF-BB, PDGF-AB, and PDGF-AA variants. The FRET responses from the analysis of PDGF-AA and PDGF-AB are much lower when compared to that from the analysis of PDGF-BB. These results are consistent with the principle of the assay. The aptamers used as affinity ligands preferentially bind to the B chain. Binding of PDGF-BB to both aptamers results in the binding-induced assembly, which generates the FRET response. Weaker binding of the aptamers to the A chain corresponds to the weaker assembly and lower FRET response.

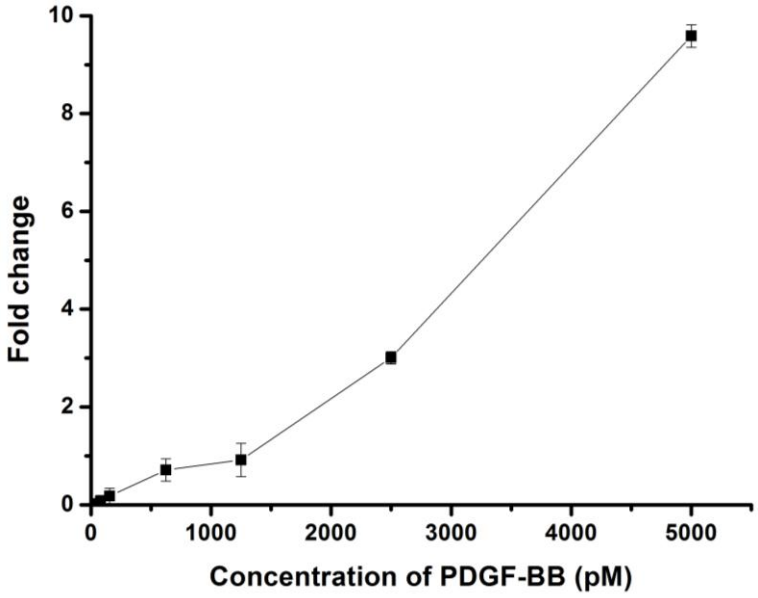

Figure 4.5 Determination of the PDGF-BB using the binding-induced FRET assay.

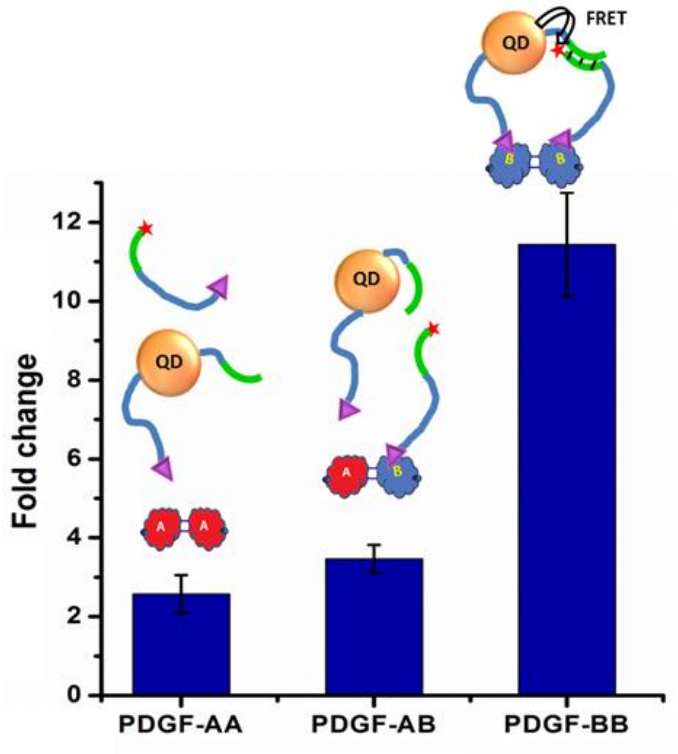

Figure 4.6 Preferential response from the detection of PDGF-BB over those from the detection of PDGF-AB and PDGF-AA.

The binding-induced DNA nanosensor is able to discriminate PDGF-BB from the PDGF-AA and PDGF-AB variants. Because the chosen two aptamers specifically binds only to the B chain of PDGF, binding of both B chains on PDGF-BB results in the formation of binding-induced DNA assembly. Binding to only one B chain (as PDGF-AB) or no binding (as in PDGF-AA) cannot form the binding-induced DNA assembly.

4.4 Conclusion

The detection of PDGF-BB and differentiation from its variants have been achieved by using the binding-induced FRET assay. The detection limit was at the pM level. Using two aptamers as affinity ligands that bind preferentially to the B chain of PDGF, the nanosensor was able to discriminate the PDGF variants. The requirement for two simultaneous binding events benefits the specificity of the assay.

The assay is not limited to the PDGF detection as shown here. In principle, this homogeneous assay can be extended to detection of other proteins provided that two affinity ligands (aptamers or antibodies) are available to bind to the protein target.

4.5 References

1. Urbain, J.L. *J. Nucl. Med.* **1999,** *40,* 498-504.

2. Alaiya, A.A.; Franzen, B.; Auer, G.; Linder, S. *Electrophoresis* **2000,** *21,* 1210-1217.

3. Disis, M.L. and M.A. Cheever, *Curr. Opin. Immunol.* **19**96, *8,* 637-642.

4. Ross, R.; Glomset, J.; Kariya, B.; Harker, L. *Proc. Natl. Acad. Sci. U. S. A.* **197**4, *71,* 1207-1210.

5. Kohler, N. and A. Lipton, *Exp. Cell Res.*, **1974,** *87,* 297-301.

6. Grotendorst, G.R.; Seppa, H. E.; Kleinman, H. K.; Martin, G. R., *Proc. Natl. Acad. Sci. U. S. A.* **1981,** *78,* 3669-3672.

7. Heldin, C.H., *EMBO J.* **1992,** *11,* 4251-4259.

8. Yarden, Y.; Escobedo, J. A.; Kuang, W. J.; Yang-Feng, T. L.; Daniel, T. O.; Tremble, P. M.; Chen, E. Y.; Ando, M. E.; Harkins, R. N.; Francke, U., et al., *Nature* **1986,** *323,* 226-232.

9. Matsui, T.; Heidaran, M.; Miki, T.; Popescu, N.; La Rochelle, W.; Kraus, M.; Pierce, J.; Pierce, J. ; Aaronson, S., *Science* **1989,** *243,* 800-804.

10. Claesson-Welsh, L. ; Eriksson, A.; Westermark, B.; Heldin, C. H., *Proc. Natl. Acad. Sci. U. S. A.* **1989,** *86,* 4917-4921.

11. Heldin, C.H.; Backstrom, G.; Ostman, A.; Hammacher, A.; Ronnstrand, L.; Rubin, K.; Nister, M.; Westermark, B., *EMBO J.* **1988,** *7*, 1387-1393.

12. Heldin, C.H.; Ernlund, A.; Rorsman, C.; Ronnstrand, L., *J. Biol. Chem.*, **1989,** *264*,8905-8912.

13. Seifert, R.A.; Hart, C. E.; Phillips, P. E.; Forstrom, J. W.; Ross, R.; Murray, M. J.; Bowen-Pope, D. F., *J. Biol. Chem.* **1989,** *264*, 8771-8.

14. Huang, C.C.; Huang, Y. F.; Cao, Z.; Tan, W.; Chang, H. T., *Anal. Chem.*, **2005,** *77,* 5735-5741.

15. Zhou, C.S.; Jiang, Y.; Hou, S.; Ma, B. ; Fang, X. ; Li, M., *Anal. Bioanal. Chem.*, **2006**. *384*: p. 1175-1180.

16. Lai, R.Y., K.W. Plaxco, and A.J. Heeger, *Anal. Chem.* **2007,** *79,* 229-233.

17. Yang, L.T.; Fung, C. W.; Cho, E. J.; Ellington, A. D., *Anal. Chem.*, **2007,** *79,* 3320-3329.

18. Li, Y.Y. ; Zhang, C.; Li, B. S.; Zhao, L. F.; Li, X. B.; Yang, W. J.; Xu, S. Q., *Clin. Chem*. **2007,** *53,* 1061-1066.

19. Green, L.S. ; Jellinek, D.; Jenison, R.; Ostman, A.; Heldin, C. H.; Janjic, N., *Biochemistry* **1996,** *35,* 14413-14424.

20. Huang, C.C. ; Chiu, S. H. ; Huang, Y. F.; Chang, H. T. *Anal. Chem.* **2007,** *79,* 4798-4804.

21. Huang, C.C. ; Chiang, C. K.; Lin, Z. H.; Lee, K. H.; Chang, H. T. *Anal. Chem.* **2008,** *80,* 1497-1504.

Chapter 5: Conclusion and Future Work

I have described in this thesis a new homogeneous assay using binding-induced fluorescence resonance energy transfer (FRET). I have developed this assay format using three examples: a model oligonucleotide sequence, a fragment of the *p53* gene encompassing a single-base mutation in codon 248, and the platelet-derived growth factor (PDGF) protein. These examples demonstrate the potential applications of the assay to the detection of specific DNA sequences, DNA mutations and specific proteins. This assay has several important advantages, as described below.

Firstly, since the assay is homogeneous, it does not require separation. In addition, the fluorescence readout is simple and fast. A very small volume of sample is required and very small amounts of reagents (QD or Cy5 labeled affinity ligands) are required for each analysis.

Secondly, the design of the assay/sensors is flexible and can be tailored to any target molecules. In principle, the sensors could be developed for any biomolecule for which a pair of affinity ligands can bind at different sites of the target molecule. Modification of the adjunct probes and capture probes with affinity ligands to QD can be readily achieved through biotin-streptavidin interaction.

Another characteristic is less obvious but equally important. To improve the detection limit, I utilized the binding-induced DNA assembly to increase the local effective concentration of the molecular components that are responsible for FRET signal generation. I optimized the experimental conditions and rationally

designed the system to minimize the target-independent assembly. The advantage of diminishing target-independent self-assembly overcomes the problem of high background that limits the ultrasensitive detection.

Potential for general application of the binding-induced strategy has been confirmed by the development of the DNA nanosensor for the detection of model DNA target, *p53* gene point mutation, and the PDGF variants. All of the above-mentioned characteristics of the sensors should allow its wide-ranging application, rapid and accurate detection with simplicity of assay operation in research and medical diagnosis.

Future research may expand to the use of different affinity ligands and targets which depend on requirements for clinical diagnosis. For example, antibodies could be used for the development of binding-induced FRET assays. Other nanomaterials and fluorescent dyes, in addition to QD and Cy5, could be incorporated into the FRET signal generation system. Further testing of the assays on real-world samples is necessary to demonstrate useful and realistic applications of the assays. Building on successful applications, additional research could include adaptation of the assays to point-of-care settings. Homogeneous assays that are simple, sensitive, and robust will have promising potential for point-of-care diagnostic applications.